Comparative Medicine
Copyright 2023
by the American Association for Laboratory Animal Science

Vol 73, No 2
April 2023
Pages 153–172

Original Research

Effects of Mouse Kidney Parvovirus on Pharmacokinetics of Chemotherapeutics and the Adenine Model of Chronic Kidney Disease

Amanda C Ritter,[1,*] Rodolfo J Ricart Arbona,[1,2] Robert S Livingston,[3] Sébastien Monette,[1,2] and Neil S Lipman[1,2,*]

Mouse kidney parvovirus (MKPV) causes inclusion body nephropathy in severely immunocompromised mice and renal interstitial inflammation in immunocompetent mice. Here we sought to determine the effects of MKPV on pre-clinical murine models that depend on renal function. To assess the effects of MKPV infection on the pharmacokinetics of 2 renally excreted chemotherapeutic agents, methotrexate and lenalidomide, we measured drug concentrations in the blood and urine of MKPV-infected or uninfected immunodeficient NOD.Cg-*Prkdc*^{scid}*Il2rg*^{tm1Wjl}/SzJ (NSG) and immunocompetent C57BL/6NCrl (B6) female mice. No differences in plasma pharmacokinetics were observed for lenalidomide. However, the AUC of methotrexate was 1.5-fold higher in uninfected NSG mice compared with infected NSG mice, 1.9-fold higher in infected B6 mice compared with uninfected B6 mice, and 4.3-fold higher in uninfected NSG mice compared with uninfected B6 mice. MKPV infection did not significantly affect the renal clearance of either drug. To assess effects of MKPV infection on the adenine diet model of chronic kidney disease, MKPV-infected and uninfected B6 female mice were fed a 0.2% adenine diet, and clinical and histopathologic features of disease were assessed over 8 wk. MKPV infection did not significantly alter urine chemistry results, hemogram findings, or serum concentrations of BUN, creatinine, or symmetric dimethylarginine. However, infection did influence histologic outcomes. As compared with uninfected mice, MKPV-infected mice had more interstitial lymphoplasmacytic infiltrates after 4 and 8 wk of diet consumption and less interstitial fibrosis at week 8. Macrophage infiltrates and renal tubular injury were similar between in infected and uninfected mice. These findings indicate that MKPV infection had minimal effects on the renal excretion of 2 chemotherapeutics and on serum biomarkers of renal function. However, infection significantly influenced two histologic features of the adenine diet model of chronic renal disease. MKPV-free mice are critically important in studies evaluating renal histology as an experimental outcome.

Abbreviations: KIM1, Kidney injury molecule 1; MKPV, mouse kidney parvovirus; NGAL, neutrophil gelatinase-associated lipocalin; SDMA, symmetric dimethylarginine

DOI: 10.30802/AALAS-CM-22-000084

Introduction

Rodent chaphamaparvovirus 1 is a novel parvovirus species that is highly divergent from previously known parvoviruses of mice, and includes murine chapparvovirus and mouse kidney parvovirus (MKPV).[43] Although MKPV was only recently discovered in research mouse colonies, the histologic characteristics of the disease it causes, inclusion body nephropathy, have been noted by pathologists for more than 40 y.[4] Inclusion body nephropathy is characterized by tubulointerstitial degenerative and inflammatory changes and intranuclear inclusions in tubular cells.[4] MKPV was discovered and demonstrated to be the causative agent of murine inclusion body nephropathy in 2018.[47] MKPV is found frequently in research mouse colonies, with an estimated prevalence of approximately 10%.[30]

MKPV replicates predominantly in renal tubular epithelium; extrarenal replication is minimal and restricted to very low copy numbers in the gastrointestinal mucosa.[25,30] Once the virus has reached the kidney, the infection is persistent and results in continuous viral replication in renal tubular epithelium and shedding of virus in urine for several months in both immunodeficient and immunocompetent mice.[16,25,47] Highly immunocompromised mice infected by MKPV develop a severe form of inclusion body nephropathy that is associated with marked histopathologic lesions in kidneys, decreased renal function, and morbidity and mortality.[25,47] Although immunodeficient mice are most severely affected, immunocompetent mice also become infected and shed virus.[16,30,47] Infection in immunocompetent mice has been demonstrated to induce persistent interstitial nephritis, although clinical signs of disease have not been documented.[16] As this virus is known to persistently replicate in murine renal tubular epithelial cells and has the potential to induce pathologic changes without overt clinical illness, infection with this virus may impact renal function and related research.[16,25]

Submitted: 17 Jul 2022. Revision requested: 21 Oct 2022. Accepted: 07 Dec 2022.
[1]Tri-Institutional Training Program in Laboratory Animal Medicine and Science, Memorial Sloan Kettering Cancer Center, Weill Cornell Medicine, and The Rockefeller University, New York, New York; [2]Center for Comparative Medicine and Pathology, Memorial Sloan Kettering Cancer Center and Weill Cornell Medicine, New York, New York; and [3]IDEXX Bioanalytics, Columbia, Missouri
**Corresponding authors: Email: carlsona@mskcc.org; lipmann@mskcc.org*

Severely immunocompromised mice, including the NOD.Cg-*Prkdc*^{scid}*Il2rg*^{tm1Wjl}/SzJ (NSG) mouse, are routinely used in oncology research as they support the growth and maintenance of a broad array of human cancer cell lines and patient-derived xenografts.[24] Therefore, NSG mice are often used to test the efficacy of emerging chemotherapeutics and combination therapies against various neoplasms, or as a patient surrogate for testing therapies in patient-derived xenografts.[24,35,41] Many chemotherapeutics depend on renal clearance. Therefore, a viral infection that impairs renal function may have substantial impact on research outcomes and may even impact patient care in the case of chemotherapy based on patient-derived xenografts.[22,67] Methotrexate and lenalidomide are chemotherapeutics commonly used to treat multiple cancers and autoimmune disorders in human patients. Both compounds are principally excreted via the renal tubules, albeit by different mechanisms. Sixty to 94% of methotrexate, an antifolate agent, is renally excreted.[29] It is actively excreted by numerous transporters (primarily OAT3 and MRP4) in the proximal renal tubular epithelium and undergoes passive reabsorption in the distal renal tubules.[22,33] Approximately 82% of lenalidomide, a thalidomide analog, is excreted primarily unchanged by kidneys by using a P-glycoprotein transporter on renal tubular epithelium.[22] Lenalidomide is not resorbed in the distal tubules nor does it bind to the OAT3 or MRP4 transporters used to excrete methotrexate.[22,29,49] Given that these compounds rely on the renal tubules for excretion and that MKPV primarily replicates in and causes damage to the renal tubules, we hypothesized that their renal excretion might be impaired in mice infected with MKPV and thus might confound studies evaluating the use of chemotherapeutics in xenografted immunocompromised mice or in immunocompetent mice engrafted with syngeneic tumors.

Murine models of renal physiology and pathophysiology allow researchers to address questions pertaining to various disease processes and help guide the development of novel therapies. The adenine diet model, which involves feeding mice a pelleted chow supplemented with 0.2% adenine, is a commonly used, well-established, murine model of chronic kidney disease (CKD).[23] This diet induces tubulointerstitial nephritis secondary to the metabolism of adenine by the enzyme xanthine dehydrogenase into 2,8-dihydroxyadenine. This causes the precipitation of crystals in the lumen of the proximal renal tubules and ascending limbs of the loops of Henle.[28,59] The resulting tubular injury leads to tubulointerstitial inflammation and fibrosis.[28,58] Qualitative and quantitative assessment of renal tubular degeneration are routinely assessed in this model.[2,45,50,58] The magnitude of fibrosis and decrease in renal function are commonly assessed by measuring serum BUN, creatinine, and phosphorus.[2,45,50,58] Symmetric dimethylarginine (SDMA) has not been assessed in the mouse adenine diet model, but as a sensitive marker of renal function in other species, it may be useful in future investigations of this and other models of renal disease in mice.[20,40] Given that MKPV, like the dietary adenine model, primarily causes tubulointerstitial lesions, MKPV might also confound research outcomes in the adenine diet model.

We conducted the current study to determine whether infection with MKPV can confound research outcomes in commonly used murine models that depend on normal renal function. We hypothesized that infection with MKPV would reduce renal clearance of the chemotherapeutic agents methotrexate and lenalidomide and that this effect would be exacerbated in an immunodeficient mouse strain. In addition, we hypothesized that, in the adenine diet model of CKD, biomarkers of renal injury such as serum BUN and creatinine would be elevated and that various histopathologic lesions would be more severe in MKPV-infected mice than in uninfected mice. In addition, this study provided the opportunity to evaluate the novel renal serum biomarker SDMA in the adenine diet model; SDMA has several advantages over serum creatinine as an indicator of renal function in other species, including greater sensitivity and independence from muscle mass, but its utility in mice has not been assessed previously.[20,40]

Materials and Methods

Animals. Female C57BL/6NCrl (B6; age, 6 to 8 wk; Charles River Laboratories, Senneville, Quebec, Canada) and NOD.Cg-*Prkdc*^{scid} *Il2rg*^{tm1Wjl}/SzJ (NSG; age, 6 to 8 wk; The Jackson Laboratory, Bar Harbor, ME) were used. All mice were free of mouse hepatitis virus, Sendai virus, mouse parvovirus, minute virus of mice, murine norovirus, pneumonia virus of mice, Theiler meningoencephalitis virus, epizootic diarrhea of infant mice (mouse rotavirus), ectromelia virus, reovirus type 3, lymphocytic choriomeningitis virus, K virus, mouse adenovirus 1 and 2, polyoma virus, murine cytomegalovirus, mouse thymic virus, hantavirus, mouse kidney parvovirus, *Mycoplasma pulmonis*, *Citrobacter rodentium*, *Salmonella* spp., *Filobacterium rodentium*, *Clostridium piliforme*, *Corynebacterium bovis*, fur mites (*Myobia musculi*, *Myocoptes musculinis*, and *Radfordia affinis*), pinworms (*Syphacia* spp. and *Aspiculuris* spp.), and *Encephalitozoon cuniculi* when the studies were initiated, as determined by testing naïve outbred Swiss Webster (Tac:SW) mice exposed repetitively to soiled bedding from cages housing mice in the colony.

Husbandry and housing. Mice were maintained in autoclaved, individually ventilated polysulfone cages with stainless-steel wire-bar lids and filter tops (no. 19, Thoren Caging Systems, Hazelton, PA) on autoclaved aspen chip bedding (PWI Industries, Quebec, Canada) at a density of no greater than 4 mice per cage. Each cage was provided with a Glatfelter paper bag containing 6 g of crinkled paper strips (EnviroPak, WF Fisher and Son, Branchburg, NJ) for enrichment. Mice were fed a natural-ingredient, closed-source, autoclavable diet (5KA1, LabDiet, Richmond, VA) or a purified diet containing 0.2% adenine (TD.140290, Envigo, Madison, WI) ad libitum. All mice received autoclaved, reverse-osmosis–purified, acidified (pH 2.5 to 2.8 with hydrochloric acid) water in polyphenylsulfone bottles with stainless-steel caps and sipper tubes (Techniplast, West Chester, PA) ad libitum. Cages were autoclaved (Century SLH Scientific, Steris, Mentor, OHOH) with a pulsed vacuum cycle of 4 pulses at a maximum pressure of 12.0 psig, with sterilization temperature of 250.5 °F (121.39 °C) for 20 min and 10.0 in. Hg vacuum dry. Sterilization was confirmed by color change of temperature-sensitive autoclave tape (Medline, Mundelein, IL) and review of the postcycle chamber conditions. Water bottles were autoclaved at a temperature of 250.0 °F (121.11 °C) for 45 min, with a purge time of 10 min. Cages were changed every 7 d within a class II, type A2 biologic safety cabinet (LabGard S602-500, Nuaire, Plymouth, MN). The rooms were maintained on a 12:12-h light:dark cycle (lights on at 0600, off at 1800), relative humidity of 30% to 70%, and room temperature of 72 ± 2 °F (22.2 ± 1.1 °C). The animal care and use program at Memorial Sloan Kettering Cancer Center is AAALAC-accredited, and all animals are maintained in accordance with the recommendations provided in the *Guide*.[21] All animal use described in this investigation was approved by Memorial Sloan Kettering Cancer Center's IACUC, in agreement with AALAS position statements on the *Humane Care and Use of Laboratory Animals* and *Alleviating Pain and Distress in Laboratory Animals*.

MKPV infection. Viral stock (MKPV substrain MSK-WCM2015-3781-1-2) was created by thawing and homogenizing frozen kidney obtained from naturally infected NSG mice with histologically and PCR-confirmed inclusion body nephritis due to MKPV infection.[30] The homogenate was resuspended in 1× PBS, passed through a sterile 0.22-µm filter (MilliporeSigma, Burlington, MA), and then centrifuged at 626 × *g* for 5 min. Supernatant was collected, aliquoted, and stored at −80 °C). This viral stock was thawed once, diluted 1:100 by using sterile PBS, aliquoted into individual portions, and stored at −80 °C until use. At inoculation, individual aliquots were thawed and administered to each mouse via oral gavage (200 µL of viral stock) and intranasally (25 µL of viral stock per nostril; total volume, 50 µL). Frozen kidney samples from mice in all sham-inoculated groups were submitted for PCR analysis to ensure that they had remained MKPV-negative for the duration of the study.

MKPV PCR. Samples were analyzed by using a validated proprietary PCR assay (IDEXX Laboratories, Columbia, MO). Total nucleic acids were extracted from kidney or urine using a commercial kit (NucleoMag Vet, Machery-Nagel, Düren, Germany). The real-time PCR assay targeted the gene coding for the MKPV NS1 protein (GenBank NC040843.1) by using a hydrolysis probe (Integrated DNA Technologies, Coralville, IA). The assay has an analytical sensitivity of between 1 and 10 template copies per PCR reaction. Analysis and amplification of the product were performed by using standard primer and probe concentrations with a commercially available master mix (LC480 ProbesMaster, Roche Applied Sciences, Indianapolis, IN) on a commercially available real-time PCR platform (LightCycler 480, Roche Applied Sciences). The copy number estimate of MKPV DNA in each PCR test was calculated by plotting the real-time crossing point values from the MKPV PCR assay on a standard curve generated by testing log-fold dilutions of a known copy-number positive control.

Pharmacokinetics study. ***Experimental design.*** Adult female NOD.Cg-*Prkdc*^{scid} *Il2rg*^{tm1Wjl}/SzJ (NSG) and C57BL/6NCrl (B6) mice (age, 6 to 8 wk; *n* = 48 per strain) were used. Mice were randomly assigned by using a random number generator (Randomizer.org) to 1 of 2 treatment groups: inoculation with MKPV (*n* = 24 mice per strain) or sham inoculation with an equivalent volume of sterile PBS (*n* = 24 mice per strain). At 10 to 11 wk after inoculation, urine was collected from each mouse and assayed for MKPV by PCR. At 14 wk after inoculation, mice (*n* = 12 per group) received a single bolus of either lenalidomide (5 mg/kg IV) or methotrexate (70 mg/kg IV) via tail vein. Blood was collected after administration of lenalidomide at 5, 15, 30, 60, 120, 240, 360, and 480 min and after methotrexate administration at 5, 15, 30, 45, 60, 90, 120, and 240 min. Blood was collected twice from each mouse: a survival collection by submental puncture and a terminal collection performed by retroorbital puncture under isoflurane anesthesia followed by euthanasia by CO_2 asphyxiation. Blood samples were collected from 3 mice at each time point and assayed for lenalidomide or methotrexate. Between the survival and terminal blood collection, mice were housed individually in cages containing hydrophobic sand (Lab Sand, Coastline Global, West Chester, PA) to facilitate urine collection. All urine excreted between the survival and terminal time points was collected for each mouse, the volume was measured, and the sample assayed for lenalidomide or methotrexate. After euthanasia, kidneys were removed, the cranial pole of the left kidney was frozen at −80 °C and retained for MKPV PCR assay, and the remaining renal tissue was preserved in 10% neutral buffered formalin for histopathology. In addition, blood collected at the terminal time point was analyzed for serum BUN, creatinine, and phosphorus.

Compound preparation. Lenalidomide (SML2283, Sigma-Aldrich, St Louis, MO) was dissolved in dimethyl sulfoxide then diluted with sterile PBS containing 1% hydrochloric acid to achieve a 1-mg/mL lenalidomide solution. Methotrexate (25 mg/mL; NDC 16729-277-30, Accord Healthcare, Durham, NC) was diluted with sterile saline to 10 mg/mL. All solutions were diluted less than 2 h prior to use and sterile-filtered by using a 0.22-µm filter (MilliporeSigma).

Pharmacokinetic quantification. Whole blood was collected into tubes containing K2EDTA anticoagulant (MiniCollect K2E K2EDTA, Greiner Bio-One, Monroe, NC) and centrifuged at 626 × *g* at 4 °C for 10 min. Plasma was decanted and placed in a preservative-free collection tube (Microcentrifuge tube, Globe Scientific, Mahwah, NJ) and stored at −80 °C until analysis. Urine was collected in preservative-free collection tubes (0.2 mL PCR Tube, Eppendorf, Hamburg, Germany) and stored at −20 °C until analysis. LC-MS analysis of thawed plasma and urine samples was performed on a triple quadrupole mass spectrometer (LCMS-8030 with LC-20AD LC pumps, Shimadzu, Kyoto, Japan). Separation was performed by using an HPLC column (Zorbax Eclipse XDB-C18 [2.1 × 50 mm, 3.5 µm], Agilent, Santa Clara, CA). Gradient separation was performed by using 0.1% formic acid in water (aqueous, A) and 0.1% formic acid in acetonitrile (organic, B) according to the following gradient (flow rate, 0.5 mL/min): 2% to 30% organic from 0 to 3 min, 2-min hold at 100% B, and 2-min return to starting conditions (2% B). Mass spectrometric detection was performed by using multiple-reaction monitoring (positive mode) of the following optimized transitions for lenalidomide and methotrexate: lenalidomide, 259.9 → 149.05 and 259.69 → 187.10; and methotrexate, 454.9 → 308.05 and 454.9 → 175.10.

Pharmacokinetic parameter calculations. Noncompartmental pharmacokinetic analysis was performed by using the linear-log trapezoidal rule for calculation of the area under the concentration–time curve (AUC_{last}) (PKanalix version 2020R1, Lixoft, Orsay, France). The pharmacokinetic parameters determined were the area under the concentration–time curve from 0 to the last observation (AUC_{last}), back-extrapolated plasma drug concentration at time zero (C_0), systemic clearance, and elimination half-life. Data points below the limit of quantification were replaced by the lower limit of quantification divided by 2. Renal clearance was calculated according to the Ae_{t1-t2}/AUC_{t1-t2} ratio, where Ae_{t1-t2} was calculated by the summation of drug excretion (urine drug concentration multiplied by urine volume) during the urine collection period from survival blood collection to terminal blood collection.[63] Urine collection intervals for methotrexate were 5 to 60 min, 15 to 90 min, 30 to 120 min, and 45 to 240 min after administration; those for lenalidomide were 5 to 120 min, 15 to 240 min, 30 to 360 min, and 60 to 480 min after administration. Mean (1 SD), geometric mean (95% CI), and coefficient of variation were calculated for each plasma pharmacokinetic parameter. Mean and 1 SD were determined for calculated renal clearances.

Clinical pathology. For serum chemistry analysis, clotted blood in serum separator tubes (MiniCollect 0.8 mL CAT Serum Separator, Greiner Bio-One) was centrifuged at 3,913 × *g* for 10 min, and the serum was decanted and stored at −80 °C until analysis. Thawed serum samples were processed by using an automated analyzer (AU680 Chemistry Analyzer, Beckman Coulter, Brea, CA) to measure the serum concentration of BUN, creatinine, and phosphorus.

Histopathology. After euthanasia of mice by CO_2 asphyxiation, complete postmortem gross examinations were performed, gross lesions were recorded, and kidneys were fixed in 10% neutral buffered formalin. After 24 to 48 h of fixation, kidneys were trimmed into 2 longitudinal and one transverse sections per mouse, processed through alcohol and xylene, paraffin-embedded, sectioned at 5 µm, and stained with hematoxylin and eosin. Renal histopathology was scored semiquantitatively as previously described.[16] In brief, slides were reviewed for tubular changes and inflammatory infiltrates, and these features were graded on a scale from 0 (within normal limits) to 4 (marked inflammatory infiltration or tubular changes). Intranuclear inclusions were noted as absent or present.

RNA in situ hybridization. Renal tissue from mice that were inoculated with but tested negative for MKPV via PCR analysis were evaluated for the presence of MKPV RNA by in situ hybridization using a target probe designed and validated to detect both viral capsid (VP1) and nonstructural (NS1) regions of MKPV.[47] Slides were stained on an automated stainer (Leica Bond RX, Leica Biosystems, Buffalo, NY) using RNAscope 2.5 LS Reagent Kit-Red (catalog no. 322150, Advanced Cell Diagnostics, Newark, CA) and Bond Polymer Refine Red Detection (catalog no. DS9390, Leica Biosystems). Control probes detecting a validated positive housekeeping gene (mouse *Ppib* to confirm adequate RNA preservation and detection; catalog no. 313918, Advanced Cell Diagnostics) and a negative bacterial gene (dapB to confirm absence of nonspecific staining; catalog no. 312038, Advanced Cell Diagnostics) were used. The chromogen was Fast Red, and sections were counterstained with hematoxylin. Positive RNA hybridization was identified as punctate chromogenic red dots under bright-field microscopy.

Adenine diet model. ***Experimental design.*** Adult female B6 mice (6 to 8 wk of age; $n = 60$) were used. Mice were randomly assigned by using a random number generator (Randomizer.org) to 1 of 2 groups: 30 mice were inoculated with MKPV, and 30 were sham-inoculated with an equivalent volume of sterile PBS. At 8 to 10 wk after inoculation, urine was collected individually from all mice and assayed for MKPV by PCR analysis to confirm infection or lack thereof. Beginning at 15 wk after inoculation, mice were fed a purified, casein-based diet containing 0.2% adenine (TD.140290, Envigo) ad libitum for a maximum of 8 wk. At 24 h prior to diet initiation (week 0), blood and urine were collected from each mouse. Mice were weighed weekly after diet initiation. On weeks 2, 4, and 8 after diet initiation, 10 mice per group were euthanized by CO_2 asphyxiation and exsanguinated via caudal vena cava puncture. CBC counts, comprehensive serum chemistry analysis, and complete gross necropsy were performed. The cranial pole of the left kidney was frozen at −80 °C and retained for MKPV PCR analysis. The remaining renal tissue was preserved in 10% neutral buffered formalin for histopathology. On weeks 0, 2, 4, 6, and 8 after diet initiation, blood was collected via submental puncture from all surviving mice, and serum BUN, creatinine, and phosphorus were quantified. In addition, serum SDMA levels were measured in all mice that survived to the 8-wk time point ($n = 20$; 10 per infection status). Two mice in the uninfected group were euthanized after the 6-wk time point but before the 8-wk time point, because they reached humane endpoint criteria. Therefore, the group size was 8 for uninfected mice at the 8-wk time point.

Clinical pathology. CBC counts were performed using an automated analyzer (ProCyte Dx Hematology Analyzer, IDEXX Laboratories) within 2 h of blood collection into tubes containing K2EDTA anticoagulant (MiniCollect K2E K2EDTA). The following parameters were determined: WBC count, RBC count, Hgb, Hct, MCV, MCH, MCHC, RBC distribution width standard deviation and coefficient of variance, relative and absolute reticulocyte counts, platelet count, platelet distribution width, mean platelet volume, and relative and absolute counts of neutrophils, lymphocytes, monocytes, eosinophils, and basophils.

For serum chemistry analysis, clotted blood collected in serum separator tubes (MiniCollect 0.8 mL CAT Serum Separator, Greiner Bio-One) was centrifuged at 3913 × *g* for 10 min. Serum was then decanted and stored at −80 °C until analysis. Thawed serum samples were processed using an automated analyzer (AU680 Chemistry Analyzer, Beckman Coulter). The following analytes were measured, depending on the experimental aim: albumin, total protein, globulin, BUN, creatinine, calcium, and phosphorus. In addition, BUN:creatinine and albumin:globulin ratios were calculated. SDMA was extracted from 20-µL samples of serum, was measured by LC-MS using calibration and quality control standards as previously described (IDEXX Laboratories).[19]

Urine collected in preservative-free tubes (0.2-mL PCR tube) was processed by using the AU680 Chemistry Analyzer to measure urine total protein and creatinine concentration. A urine total protein:creatinine concentration ratio was calculated. Urine specific gravity was measured by using a refractometer (TS Meter Refractometer, Leica).

Histopathology. After euthanasia by CO_2 asphyxiation, mice underwent a complete postmortem gross examination. Gross lesions were recorded, and all tissues were fixed in 10% neutral buffered formalin. After 24 to 48 h of fixation, kidneys were trimmed into 2 longitudinal and one transverse sections per mouse, processed through alcohol and xylene, paraffin-embedded, sectioned at 5 µm, and stained with hematoxylin and eosin and with Sirius Red (for collagen).

Renal lesions in the sections stained with hematoxylin and eosin were scored using a semiquantitative method that assessed the following features: 1) the extent of tubular degeneration (estimated as the percentage of tubules with degenerative changes [including epithelial basophilia, vacuolation, attenuation, and necrosis] evaluated at 4× magnification using the following scoring scale: 0, 0%; 1, 1% to 50%; 2, 51% to 60%; 3, 61% to 70%; 4, 71% to 80%; 5, 81% to 90%; and 6, 91% to 100%); 2) number of tubules with intratubular inflammation in ten 10× fields; 3) total number of interstitial lymphoplasmacytic infiltrate foci visible at 4× in the 3 whole sections, 4) total number of mineralized tubules visible at 4× on the 3 whole sections, and 5) number of adenine crystals in ten 10× fields.

Two investigators (AR and SM) who were blind to group and who used different microscopes (AR: Olympus BX61; SM: Olympus BX45) scored all samples. The average of the 2 scores was reported. The extent of fibrosis was quantified on whole-slide images of Sirius Red–stained sections acquired under polarized light by using a dual CCD camera with a 20×/0.8 NA objective (Olympus BX61 microscope, DP80 camera, CellSens Dimension [version 3.2] software, Tokyo, Japan), resulting in an image resolution of 0.51 µm/pixel. The proportion of renal tissue exhibiting birefringence (excluding the renal pelvis, capsule, and interlobar vessels) was quantified by using image analysis software (QuPath v0.3.0 thresholder algorithm, Queen's University, Belfast, Northern Ireland).[3]

Immunohistochemistry. Immunohistochemistry was performed on kidney sections by using an automated stainer and system reagents (Leica Bond RX, Leica Biosystems). Immunohistochemistry stains were selected on the basis of their routine use in published studies of the adenine diet model

and included the F4/80 stain for murine macrophages and the KIM1 and NGAL stains for renal tubular injury.[9,28,51,60,64,65] After deparaffinization and heat-induced epitope retrieval in a citrate pH 6.0 buffer (F4/80, KIM1) or EDTA pH 9.0 buffer (NGAL), immunohistochemistry for F4/80, KIM1, and NGAL was performed by using the following primary and secondary antibodies: Invitrogen catalog no. 14-4801-85 (dilution, 1:100) and Vector Laboratories catalog no. BA-4001 (1:100); R and D Systems catalog no. AF1817 and Vector Laboratories catalog no. BA-5000 (1:1000); Invitrogen catalog no. PA5-79590 and Leica Biosystems catalog no. DS9800 reagent 3 (used at the concentration provided by vendor), respectively, and then a polymer detection system (DS9800, Leica Biosystems). The chromogen was 3,3 diaminobenzidine tetrachloride, and sections were counterstained with hematoxylin. Slide image acquisition was performed as described for Sirius Red–stained sections, except without polarized light. The proportion of tissue area positive for DAB was quantified by using image analysis software (QuPath version 0.3.0 thresholder algorithm, Queen's University, Belfast, Northern Ireland).[3]

Statistical analysis. For the pharmacokinetic study, drug concentration at each time point and pharmacokinetic parameters (AUC_{last}, C_0, systemic clearance, elimination half-life) were compared by 2-way ANOVA for the variables of strain and infection status. Clinical and histopathology outcomes were compared by 3-way ANOVA for the variables of drug, strain, and infection status. Renal clearance was compared by 3-way ANOVA for the variables of collection interval, strain, and infection status. If the 3-way ANOVA showed that collection interval was not a significant factor, it was excluded as a variable, and 2-way ANOVA was then performed for strain and infection status. Posthoc analysis was performed using the Tukey multiple comparison test. For the adenine diet model, body weight, serum BUN, creatinine, phosphorus, SDMA, and all urine chemistry parameters were assessed by using a repeated-measures mixed-effects model of infection and time after diet initiation. Posthoc analysis was performed using the Sidak multiple comparison test. The Pearson correlation coefficient was used to determine correlation between SDMA and creatinine. Data that were collected only at terminal time points, including histopathologic outcomes (except extent of tubular degeneration), renal weight, CBC, and complete serum chemistry, were assessed by 2-way ANOVA for the variables of infection and time after diet initiation. Posthoc analysis was performed using the Tukey multiple comparison test. Ordinal data (histopathologic semiquantitative scoring) was analyzed by using the Mann–Whitney *U* test for both pharmacokinetic and adenine diet aims. All analyses were performed by using statistics software (Prism 9.1.0, Graph Pad Software, La Jolla, CA). A P value of less than or equal to 0.05 denoted statistical significance.

Results

Pharmacokinetics. ***MKPV infection.*** All urine and kidney samples collected from sham-inoculated mice (n = 48) at 10 wk after inoculation and at euthanasia were PCR negative for MKPV. Urine collected from NSG mice at 11 wk after inoculation was positive for MKPV in 14 of 24 (58%) of inoculated mice. In contrast, all (n = 24) B6 mice that were inoculated for MKPV had PCR-positive urine by 11 wk after inoculation. Kidneys were assayed for MKPV at 14 wk after inoculation, with 6 additional MKPV-inoculated NSG mice testing positive, resulting in an overall infection rate of 83% (20 MKPV positive of 24 mice). The 4 MKPV-negative NSG mice, comprised of 1 mouse given methotrexate and 3 given lenalidomide, were excluded from pharmacokinetic and pathologic analysis. MKPV RNA was not detected in PCR-negative kidneys based on in situ hybridization.

Histopathology. The histopathology scores assigned to renal tissues are shown in Figure 1. Drug administered was not a significant factor as determined by 3-way ANOVA and therefore was not included as a variable. Four MKPV-inoculated but PCR-negative NSG mice had no inclusion bodies and therefore were not scored for histologic changes. One B6 mouse inoculated with MKPV spontaneously died for reasons unrelated to the

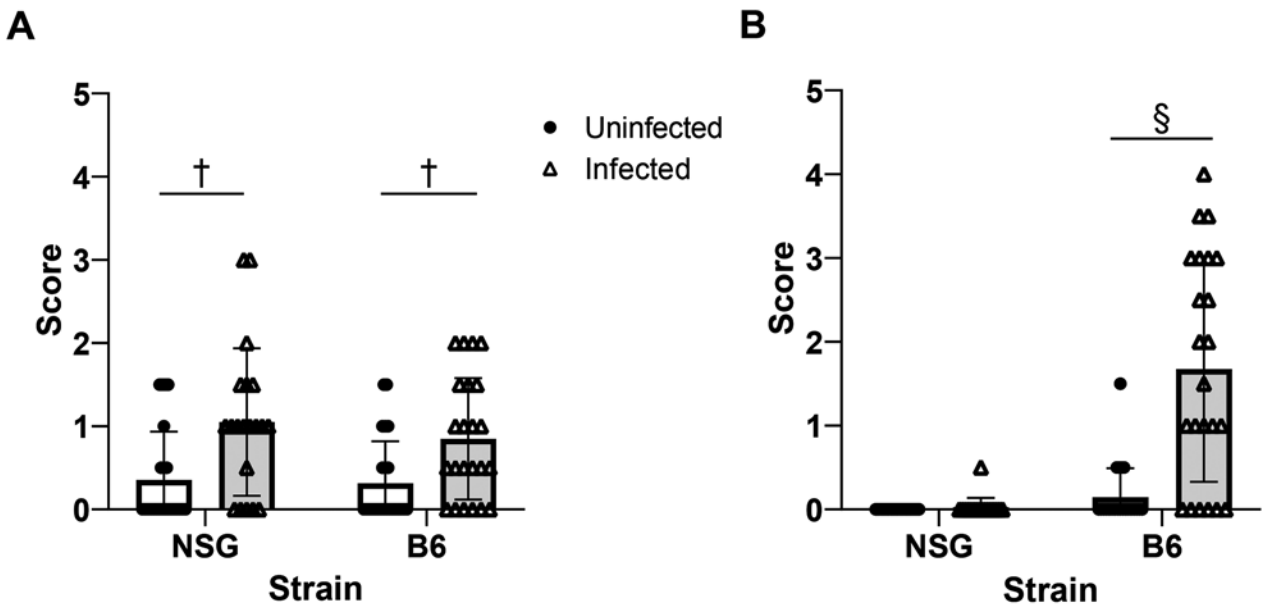

Figure 1. Semiquantitative scoring of (A) tubular degeneration and (B) interstitial inflammation at 14 wk after inoculation in NSG and B6 uninfected (closed circle) and infected (open triangle) mice independent of drug administration. Data displayed as mean (bar) ± 1 SD (error bars) with individual animals (symbols). All groups contained 24 mice, except for infected NSG mice (n = 20) and infected B6 mice (n = 23). †, $P < 0.005$; §, $P < 0.0001$.

study; its kidneys were not assessed. Infected B6 mice had more extensive ($P < 0.0001$) interstitial lymphoplasmacytic infiltrates than did uninfected B6 mice. Tubular degeneration was more severe in MKPV-infected as compared with sham-inoculated NSG ($P = 0.0046$) and B6 ($P = 0.0046$) mice. Although this result was statistically significant, the magnitude of the change was mild; the mean score assigned to infected NSG mice was only 1.1, representing minimal pathology. Inclusion bodies were present in the proximal renal tubular epithelium of 11 of 20 (55%) MKPV-positive NSG mice, whereas only 1 of the 23 (4%) MKPV-positive B6 mice had inclusion bodies.

Clinical pathology. The serum chemistry values from blood samples collected at euthanasia are shown in Table 1. Serum BUN was significantly higher in mice receiving methotrexate as compared with lenalidomide ($F_{1,83} = 86.33$, $P < 0.0001$]). Methotrexate-treated, MKPV-infected NSG mice had higher serum BUN ($P = 0.003$) and creatinine ($P = 0.03$) than did methotrexate-treated, MKPV-infected B6 mice. Methotrexate-treated, MKPV-infected B6 mice had lower serum creatinine than uninfected B6 mice receiving the same drug ($P = 0.0165$). Neither strain, drug, nor infection status affected serum phosphorus concentration.

Methotrexate pharmacokinetics. Plasma concentrations of methotrexate are shown in Figure 2. One NSG mouse inoculated with MKPV was PCR negative and thus was excluded from analysis, eliminating a data point at 45 and 240 min after drug administration for this group. The plasma concentration of methotrexate was higher in uninfected than infected NSG mice at 5 ($P = 0.0006$) and 15 ($P = 0.04$) min after injection. The plasma concentration of methotrexate was higher ($P = 0.01$) in infected than uninfected B6 mice at 5 min after injection. The plasma concentration of methotrexate was higher in uninfected NSG compared with uninfected B6 mice at 5 ($P < 0.0001$), 15 ($P = 0.002$), 30 ($P < 0.0001$), 45 ($P = 0.009$), and 60 ($P = 0.0009$) min after injection.

Noncompartmental pharmacokinetic parameters for methotrexate are shown in Table 2. AUC_{last} was higher in uninfected compared with infected NSG mice ($P < 0.0001$), infected compared with uninfected B6 mice ($P < 0.0001$), and uninfected NSG mice compared with uninfected B6 mice ($P < 0.0001$). AUC_{last} was 1.5 times higher in uninfected NSG mice compared with infected NSG mice, 1.9 times higher in infected B6 mice compared with uninfected B6 mice, and 4.3 times higher in uninfected NSG mice compared with uninfected B6 mice. The extrapolated initial concentration (C_0) was higher in uninfected NSG mice than in infected NSG mice ($P = 0.03$) and uninfected B6 mice ($P = 0.0001$). Clearance took longer in uninfected B6 mice as compared with infected B6 mice ($P = 0.0009$) and uninfected NSG mice ($P < 0.0001$). Drug half-life did not differ between strains or infection status.

Renal clearance data for mice given methotrexate are shown in Table 3. Renal clearance was significantly influenced by collection period ($F_{3,23} = 3.705$, $P = 0.0261$). Therefore, renal clearance data was analyzed with collection period as a variable. Because of the short time intervals, mice that had urine collected from 5 through 60 min or 15 through 90 min after administration often failed to produce sufficient urine for methotrexate quantification; therefore renal clearance data for these intervals were excluded from analysis. Renal clearance of methotrexate did not differ between infected and uninfected mice of either strain, whereas mouse strain—but not infection status—was a significant source of variation for methotrexate renal clearance ($F_{1,15} = 11.25$, $P = 0.0043$). Renal clearance, in general, took longer in B6 than NSG mice, but posthoc analysis failed to detect statistically significant differences between strains for either specific collection interval.

Lenalidomide pharmacokinetics. The postinjection plasma concentrations of lenalidomide are shown in Figure 3. Three inoculated NSG mice were excluded from analysis because they were PCR-negative for MKPV at the end of the study, leading to the exclusion of one data point each at 5, 30, 60, 120, 360, and 480 min after drug administration for this group. In addition, one MKPV-inoculated B6 mouse was found dead prior to lenalidomide administration and was excluded from analysis, causing the elimination of one data point each at 30 and 360 min after drug administration for this group. Plasma lenalidomide concentrations did not differ between infected and uninfected mice at any time point. At 480 min after injection, plasma lenalidomide concentration was higher ($P = 0.0079$) in uninfected NSG mice than uninfected B6 mice. None of the noncompartmental pharmacokinetic parameters for lenalidomide (Table 4) differed between mice based on infection status or strain.

Renal lenalidomide clearance data are shown in Table 3. Because renal clearance of lenalidomide was not influenced by time, collection period was not evaluated as a variable. Lenalidomide renal clearance did not differ between infected and uninfected mice of either strain. However, strain was a significant source of variation ($F_{1,39} = 25.29$, $P < 0.0001$), and uninfected NSG mice had significantly slower renal clearance than did uninfected B6 mice ($P < 0.0001$).

Adenine diet. *MKPV infection.* All samples of urine and renal tissue collected from sham-inoculated mice ($n = 30$) at 10 wk after inoculation and at euthanasia were MKPV PCR negative.

Table 1. Serum chemistry analytes at 14 wk after infection in NSG and B6 mice given methotrexate or lenalidomide

Drug	Strain	Infection status	BUN (mg/dL)	Creatinine (mg/dL)	Phosphorus (mg/dL)
Methotrexate	NSG	Uninfected	35 ± 5[c]	0.32 ± 0.09	11.3 ± 1.5
		Infected	39 ± 5[b,c]	0.33 ± 0.07[b]	12.4 ± 2.2
	B6	Uninfected	34 ± 4[c]	0.33 ± 0.07[a]	13.0 ± 1.9
		Infected	32 ± 6[b,c]	0.25 ± 0.03[a,b]	11.3 ± 1.2
Lenalidomide	NSG	Uninfected	27 ± 5[c]	0.30 ± 0.06	11.8 ± 1.6
		Infected	24 ± 3[c]	0.26 ± 0.03	11.5 ± 1.8
	B6	Uninfected	25 ± 4[c]	0.26 ± 0.07	11.7 ± 1.7
		Infected	25 ± 4[c]	0.23 ± 0.03	11.7 ± 1.3

Data are displayed as mean ± 1 SD.
Group size: $n = 12$, except for infected NSG mice administered methotrexate ($n = 11$), infected B6 mice administered lenalidomide ($n = 11$), and infected NSG mice administered lenalidomide ($n = 9$)
[a]$P < 0.05$ between uninfected and infected mice of the same strain and given the same drug
[b]$P < 0.05$ between NSG and B6 mice of the same infection status and given the same drug
[c]$P < 0.05$ between mice given different drugs but of the same infection status and strain.

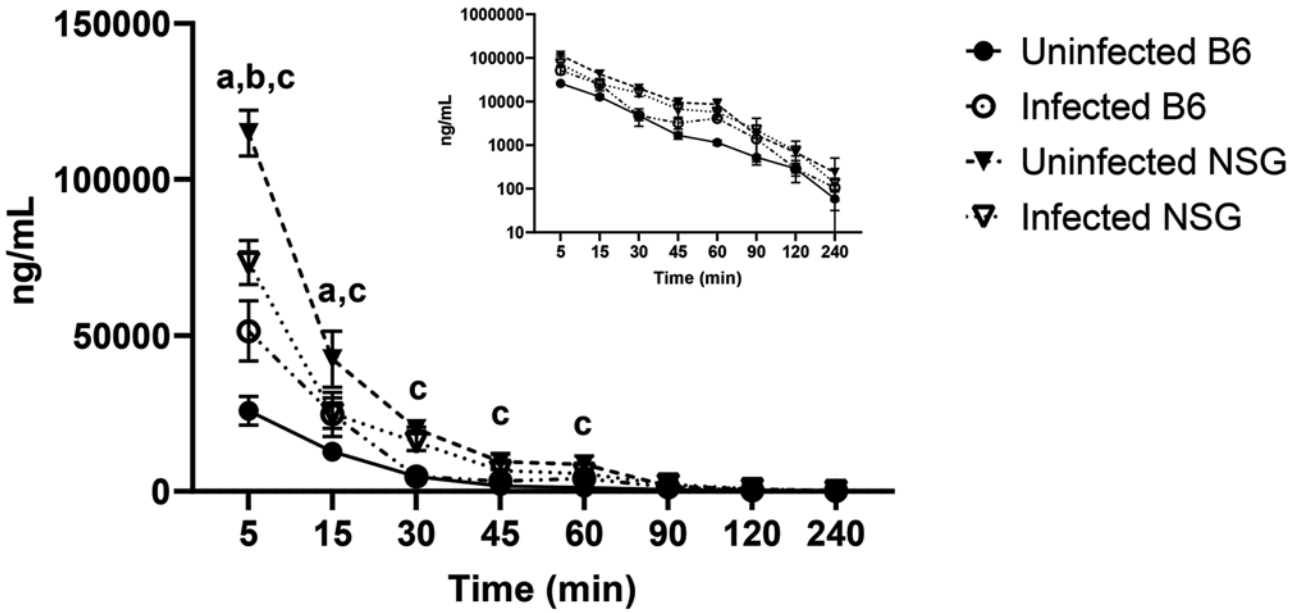

Figure 2. Plasma concentrations of methotrexate in uninfected (filled) and infected (open) B6 (circles) or NSG (triangles) mice 14 wk after inoculation. Inset, log-transformed plasma concentrations. Data are displayed as mean ± 1 SD; all groups contained 3 mice, except for infected NSG mice at 45 and 240 min ($n = 2$). a, $P < 0.05$ between infected and uninfected NSG mice; b, $P < 0.05$ between infected and uninfected B6 mice; c, $P < 0.05$ between uninfected NSG and B6 mice.

In contrast, all urine samples collected from MKPV-inoculated B6 mice ($n = 30$) were MKPV PCR positive by 11 wk after inoculation.

Body and kidney weight. Both total body weight and renal weight declined after initiation of the adenine diet. However, no significant differences were detected in body or renal weight of infected as compared to uninfected mice at any time point (Figure 4 A and B).

Clinical pathology. Serum chemistry analytes are shown in Figure 4 C through F and Table 5. Two mice in the uninfected group died between the 6- and 8-wk time points; therefore, the uninfected group size was only 8 at week 8. Infection status did significantly affect serum BUN, phosphorus, or SDMA at all time points. Serum creatinine was higher in uninfected mice at baseline ($P = 0.034$) and at week 2 ($P = 0.0021$) as compared with infected mice. At 6 wk after diet initiation, serum creatinine was higher ($P = 0.003$) in MKPV-infected mice than in uninfected mice; this difference was not present at 8 wk. Other serum chemistry parameters were not significantly different between infected and uninfected mice at any time point. Creatinine and SDMA values were strongly correlated ($r = 0.68$, $P < 0.0001$).

None of the CBC parameters (Table 6) differed between uninfected and infected mice at any time point. Duration of diet administration—but not infection status—was an important source of variation for multiple parameters. The absolute reticulocyte count increased significantly from week 2 to 8 in both uninfected ($P = 0.0001$) and infected ($P = 0.0002$) mice, whereas Hct decreased from week 2 to 8 in both uninfected ($P < 0.0001$) and infected ($P = 0.0009$) mice. Infection status had no effect on either of these parameters, and infected mice were not different from uninfected mice at any time point.

Urine chemistry. Neither urine specific gravity, creatinine, total protein, nor the total protein:creatinine ratio differed between infected and uninfected mice at any time point (Figure 5). All urinary parameters decreased significantly after adenine diet initiation.

Histopathology. ***Hematoxylin and eosin staining.*** Representative photomicrographs of lesions observed after 8 wk of adenine diet consumption are provided in Figure 6 A through D. The scoring results for histologic features observed in the adenine diet study are provided in Figure 7. Neither the extent of tubular degeneration, intratubular inflammation, mineralization, nor number of adenine crystals differed between infected and uninfected mice at any time point (Figure 7 A, B, D, and E). The number of interstitial lymphoplasmacytic infiltrates was higher in infected than in uninfected mice at all time points (Figure 7 C). This difference was statistically significant at 4 wk ($P < 0.0001$) and 8 wk ($P < 0.0001$) after diet initiation.

Sirius red staining. Representative photomicrographs of Sirius red-stained whole-kidney sections after 8 wk of adenine diet consumption are provided in Figure 6 E and F. The quantification of renal collagen is provided in Figure 8 A. Interstitial fibrosis increased over time but did not differ significantly between infected and uninfected mice at 2 and 4 wk after adenine diet initiation. At 8 wk, infected mice had less ($P = 0.0009$) interstitial fibrosis than did uninfected mice.

Immunohistochemistry. Representative photomicrographs of immunohistochemically stained tissue sections are provided in Figure 6 G and H and Figure 8. The quantification of the DAB-positive areas as a percentage of the total renal tissue area is provided in Figure 9. No significant differences in DAB-positive areas were detected between infected and uninfected mice at any time point for F4/80, KIM1, or NGAL. Both infected and uninfected mice showed significantly less KIM1 staining over time ($F_{2,52} = 117.1$, $P < 0.0001$).

Discussion

All B6 mice inoculated with MKPV were PCR positive by 10 to 11 wk after inoculation. Several (4 of 24, 17%) of the inoculated NSG mice had not become infected by 14 wk after inoculation, based on urine and renal PCR analysis and renal in situ hybridization. In our experience with this MKPV infection model, this inoculation dose and route results in infection detectable by PCR on urine samples in a high proportion of B6 and NSG mice at 10 wk after inoculation and in early histopathologic renal

Table 2. Noncompartmental pharmacokinetic parameters of methotrexate in uninfected and MKPV-infected B6 and NSG mice at 14 wk after infection

	B6						NSG					
	Uninfected			Infected			Uninfected			Infected		
	Geometric mean	95% CI	%CV	Geometric mean	95% CI	%CV	Geometric mean	95% CI	%CV	Geometric mean	95% CI	%CV
AUC_{last} (min × ng/mL)	603,460[a,b]	409,423–889,456	16.25	1,169,612[a]	1,146,500–1,193,189	0.80	2,621,271[a,b]	2,544,772–2,700,069	1.20	1,778,095[a]	1,551,174–2,038,212	5.49
C_0 (ng/mL)	36,331[b]	21,300–61,970	22.30	73,839	26,777–203,617	35.23	189,968[a,b]	140,196–257,410	11.87	125,527[a]	77,726–202,725	18.23
Cl (mL/min)	3.10[a,b]	1.90–5.05	18.45	1.56[a]	1.31–1.86	7.03	0.70[b]	0.68–0.73	1.43	1.04	0.88–1.23	6.73
$t_{1/2}$ (min)	43.86	25.38–75.79	22.30	40.26	19.78–81.93	30.49	34.10	25.06–46.40	12.78	28.39	8.13–99.15	52.71

AUC_{last}, AUC from time zero to the last observation (240 min after injection); C_0, back-extrapolated plasma drug concentration at time zero; Cl, systemic clearance; CV, coefficient of variation; $t_{1/2}$, elimination half-life

[a] $P < 0.05$ between infected and uninfected mice of the same strain

[b] $P < 0.05$ between uninfected B6 and NSG mice

changes at 14 to 15 wk.[25] These results were the basis for the selection of this time point to conduct pharmacokinetics analysis and to initiate the adenine diet studies. However, we also have observed that although effects of the infection are more severe in NSG than B6 mice in late infection (5-6 mo), the onset of viral shedding tends to occur later and the amount of virus shed in urine tend to be lower in NSG mice as compared with B6 mice in the early stage (prior to 5 mo) of infection.[25] The mechanism underlying this difference has not been determined. The only sites other than the kidney in which MKPV replication has been documented are hepatocytes and cells in the gastrointestinal lamina propria.[16,30] Although viral replication at these sites appeared to be minimal compared with replication in renal tubules, these sites may be important in early infection after oral exposure before the virus reaches the kidney. A possible explanation for the delayed shedding during the early stage of infection in NSG mice is a paucity of the cells that support initial viral replication in the gastrointestinal tract of NSG as compared with B6 mice. These cells may be of immune origin and thus may be low or absent in NSG mice. Murine astrovirus 2 is a recent example of a virus that appears to require immune cells to perpetuate infection, because it does not infect NSG mice.[46]

MKPV infection was not associated with significant differences in serum BUN or creatinine concentrations in mice given chemotherapeutics at 14 wk after inoculation, with the exception that methotrexate-treated, MKPV-infected B6 mice had significantly lower serum creatinine concentrations than uninfected B6 mice. These results indicate that MKPV infection did not result in overt impairment of kidney function in either strain under our experimental conditions. All groups of mice given methotrexate had higher serum BUN concentrations than mice given lenalidomide, but creatinine did not increase concomitantly. Elevations in BUN, without a corresponding increase in serum creatinine, can result from proximal gastrointestinal bleeding.[17] Administration of methotrexate has been documented to cause gastrointestinal mucosal injury in humans and mice, although these adverse events are typically associated with chronic administration.[12,62] In the present study, a maximum of 4 h separated administration of methotrexate and blood collection. Microscopic examination of the gastrointestinal tract was not performed, and therefore we cannot comment on the possible presence of gastrointestinal mucosal damage.

Significant differences in AUC_{last} (both strains), clearance (B6 mice only), and C_0 (NSG mice only) of methotrexate occurred in MKPV-infected mice as compared with uninfected mice of the same strain. However, half-life was not affected in either strain, suggesting that changes in the volume of distribution are likely the major contributor to the differences in clearance and C_0.[36] Potential mechanisms for a reduced volume of distribution that would result in decreased clearance in the MKPV-infected B6 group include dehydration and increased drug–protein binding. Both conditions can occur in disease, but increased drug–protein binding in particular can occur during a proinflammatory state associated with systemic infection.[37] MKPV-infected NSG mice had lower C_0 than uninfected mice, suggesting a higher volume of distribution. Capillary leakage or decreased drug protein binding are potential causes of increases in volume of distribution. Viral infection can induce endothelial permeability through various cytokine pathways or cause direct endothelial damage.[14,34,52] The possibility of vascular permeability contributing to alterations in the volume of distribution in response to infection in the NSG strain is unclear as the *IL2rg*^{null} mutation reduces cytokine signaling through multiple receptors.[53,68] To our knowledge, endothelial damage secondary to MKPV infection has not been assessed.

Table 3. Renal clearance (mL/min) of methotrexate or lenalidomide in uninfected and MKPV-infected B6 and NSG mice 14 wk after infection

Drug	Collection interval (min)	B6		NSG	
		Uninfected	Infected	Uninfected	Infected
Methotrexate	45–240	1.87 ± 1.84	1.49 ± 1.62	0.06 ± 0.02	0.19 ± 0.04
	30–120	0.39 ± 0.16	0.35 ± 0.32	0.06 ± 0.02	0.49 ± 0.09
Lenalidomide	All	0.42 ± 0.27[a]	0.27 ± 0.18	0.02 ± 0.02[a]	0.11 ± 0.11

Data presented as mean ± 1 SD.
[a]$P < 0.05$ between uninfected B6 and NSG mice.

Although alterations in AUC between infected and uninfected mice dosed with methotrexate were statistically significant, the biologic significance of the differences is less clear. FDA guidance suggests that at least a 2-fold change in AUC is necessary to be considered biologically relevant.[6,7,66] The difference in AUC between uninfected and infected mice of either strain was less than 2-fold. In addition, renal clearance of methotrexate did not differ between infected and uninfected mice. Renal clearance is typically considered a constant rate when drugs undergo linear kinetics; in contrast, methotrexate excretion depends on saturable resorption and secretion pathways, perhaps explaining why clearance was significantly impacted by the collection interval.[18] Despite statistically significant differences in the AUC_{last} and clearance or C_0 of methotrexate between infected and uninfected mice, MKPV-induced alterations in renal clearance were likely not the etiology, contrary to our initial hypothesis. Without examining pharmacodynamics, one cannot definitively determine whether the alterations in AUC are biologically relevant. Differences in the growth kinetics of methotrexate-susceptible tumors might be examined to determine biologic relevance.

Lenalidomide plasma pharmacokinetics did not differ between infected and uninfected mice of the same strain, suggesting that alterations in AUC, clearance, and C_0 in infected mice are drug dependent. In humans, lenalidomide AUC, half-life, and renal clearance did not differ between patients with mild renal impairment and those with normal renal function but were altered in patients with moderate and severe renal impairment.[10] The clinical and anatomic pathology findings of the current study indicate that the mice evaluated have early or no functional renal impairment. Although methotrexate and lenalidomide have different mechanisms of renal excretion, neither drug showed differences in renal clearance between MKPV-infected mice and uninfected controls. This finding suggests that MKPV infection did not significantly alter either renal clearance mechanism. The effect of MKPV infection on other factors that influence plasma pharmacokinetics, including plasma protein binding, drug metabolism, and nonrenal excretion and which differ between methotrexate and lenalidomide, may have contributed to the difference in the influence of MKPV infection on plasma pharmacokinetics.

We noted significant interstrain differences in drug disposition, particularly among mice given methotrexate. Uninfected NSG and B6 mice receiving methotrexate differed significantly in AUC_{last}, C_0, and clearance, but not in half-life. However, the magnitude of the difference in half life was larger between uninfected B6 and NSG mice than between infected and uninfected mice of either strain. Significant changes in the volume of distribution along with changes in AUC or clearance may mask changes in half-life.[5] The renal clearance of lenalidomide differed with regard to strain but not infection status. Possible explanations for these interstrain pharmacokinetic differences may include differences in plasma protein concentrations or drug binding, which in turn can influence the volume of distribution and renal clearance of drugs.[54] A study comparing

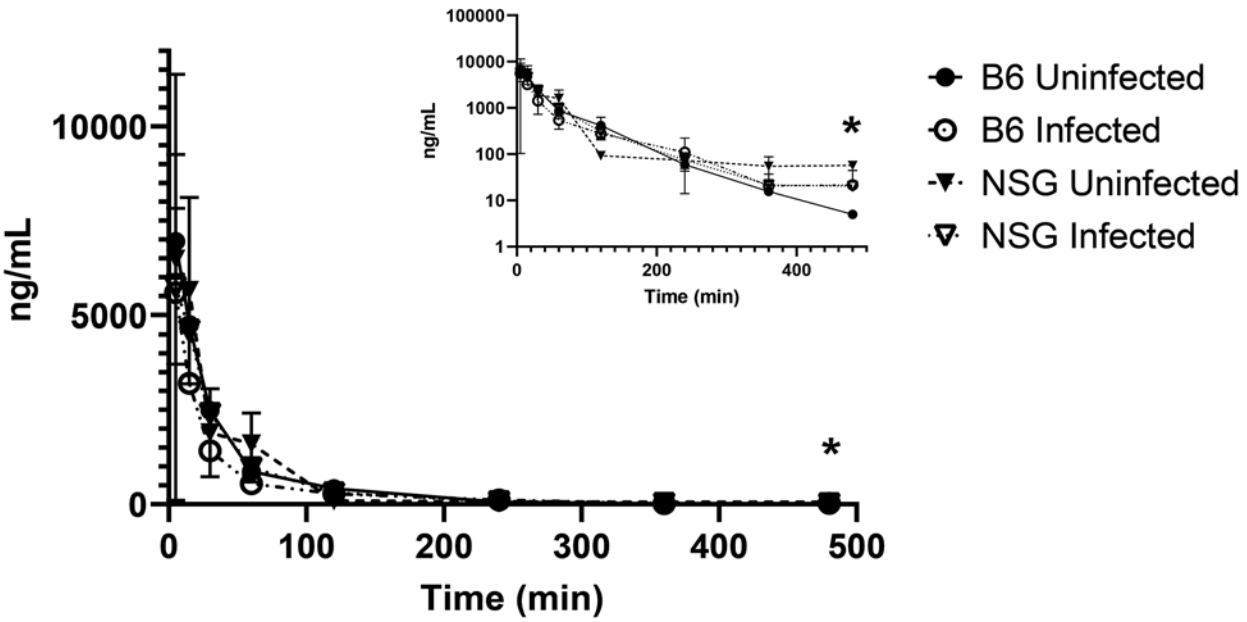

Figure 3. Plasma concentrations of lenalidomide in uninfected (filled) or infected (open), B6 (circles) or NSG (triangles) mice at 14 wk after inoculation. Inset, log-transformed plasma concentrations. Data are displayed as mean ± 1 SD; all groups contained 3 mice, except for infected NSG mice at 5, 30, 60, 120, 360, and 480 min and infected B6 mice at 30 and 360 min ($n = 2$). *, $P < 0.05$ between uninfected NSG and B6 mice.

Table 4. Noncompartmental pharmacokinetic parameters of lenalidomide in uninfected and MKPV-infected B6 and NSG mice at 14 wk after infection

	B6						NSG					
	Uninfected			Infected			Uninfected			Infected		
	Geometric mean	95% CI	%CV	Geometric mean	95% CI	%CV	Geometric mean	95% CI	%CV	Geometric mean	95% CI	%CV
AUC_{all} (min × ng/mL)	273,301	220,295–339,061	8.89	209,157	160,850–271,971	10.87	282,646	240,166–331,712	6.41	290,563	191,530–440,802	16.75
C_0 (ng/mL)	8348	5,333–13,068	18.82	7387	7282–7494	0.58	7429	1,336–41,301	53.89	6126	398–94,289	73.68
Cl (mL/min)	0.50	0.40–0.63	8.72	0.61	0.45–0.82	11.82	0.48	0.39–0.60	8.61	0.47	0.32–0.68	14.84
$t_{1/2}$ (min)	41.21	33.83–50.19	8.11	75.01	53.90–104.4	12.82	69.75	55.95–86.96	8.98	64.66	22.93–182.3	44.29

AUC_{last}, AUC from time zero to the last observation (480 min after injection); C_0, back-extrapolated plasma drug concentration at time zero; Cl, systemic clearance; CV, coefficient of variation; $t_{1/2}$, elimination half-life

plasma protein profiles of 5 mouse strains found similar plasma protein profiles across all sexes and strains, including C57BL/6 and NOD/SCID mice.[39] Although that study did not assess the plasma protein profile of the NSG mice, they are closely related to NOD/SCID mice, differing only in the IL2rg mutation.[53] Therefore, B6 and NSG mice likely have similar plasma protein profiles in health; how or whether infection alters the plasma protein profiles of these strains has not been determined. Although the mechanisms underlying the differences in pharmacokinetics are unclear, the observed interstrain differences suggest that pharmacokinetic data should not be extrapolated readily between mouse strains. NSG mice are known to have significant differences in the pharmacokinetic profiles of antibody and antibody–drug conjugates as compared with BALB/c, athymic nude, and SCID mice, resulting in reduced antitumor activity of the tested compounds.[31] The mechanism responsible for the alterations in pharmacokinetic properties of antibodies is likely different than that underlying the results of the present study. Our results show that differences in mouse strain can significantly alter pharmacokinetics of test agents. Therefore, studies investigating pharmacokinetic or toxicokinetic properties of various compounds should use mice of the same strain.

Our current pharmacokinetic study had several limitations. First, several NSG mice were removed from analysis because they did not become infected, thus resulting in several time points for which fewer mice contributed to the pharmacokinetic data, particularly for NSG mice given lenalidomide. This resulted in increased intragroup variability. In addition, we did not assess pharmacodynamic end points that would have enhanced our understanding of the biologic significance of the alterations in pharmacokinetic parameters. The histologic changes of MKPV infection were relatively mild in inoculated mice. Mice that are at a later stage of infection or have more severe pathology (as commonly occurs in older NSG mice after prolonged infection) may have alterations in pharmacokinetics that were not yet apparent here. We used only female mice, as was done in prior studies that temporally evaluated MKPV pathogenesis.[25] The applicability of our current data to other strains of MKPV, later stages of MKPV infection, other strains and sexes of mice, and other drugs requires further study.

In the adenine diet–induced model of chronic kidney disease, all inoculated mice became infected prior to induction of the model, and induction of the model was successful in both groups, with infected and uninfected mice developing azotemia, hyperphosphatemia, anemia, and hyposthenuria relative to baseline, as previously reported in other studies using this model.[23,28,59] MKPV infection for longer than 15 wk did not significantly worsen measurable clinicopathologic parameters in female C57BL/6NCrl mice; this outcome was contrary to our hypothesis that infection would worsen renal functional biomarkers in this model. Neither serum BUN, phosphorus, nor SDMA differed between infected and uninfected mice at any time point. Creatinine was significantly higher in uninfected mice at 2 time points, but the absolute difference between groups was not clinically significant. At 6 wk after diet administration, infected mice had significantly higher creatinine than did uninfected mice. No corresponding elevations in serum SDMA or BUN, which would suggest a reduced glomerular filtration rate, were detected in infected mice at this time point. Serum samples from infected and uninfected mice were processed for serum creatinine, BUN and phosphorus in the same analyzer run. Due to concerns regarding the serum creatinine results, analysis was repeated on the same serum samples, but repeat

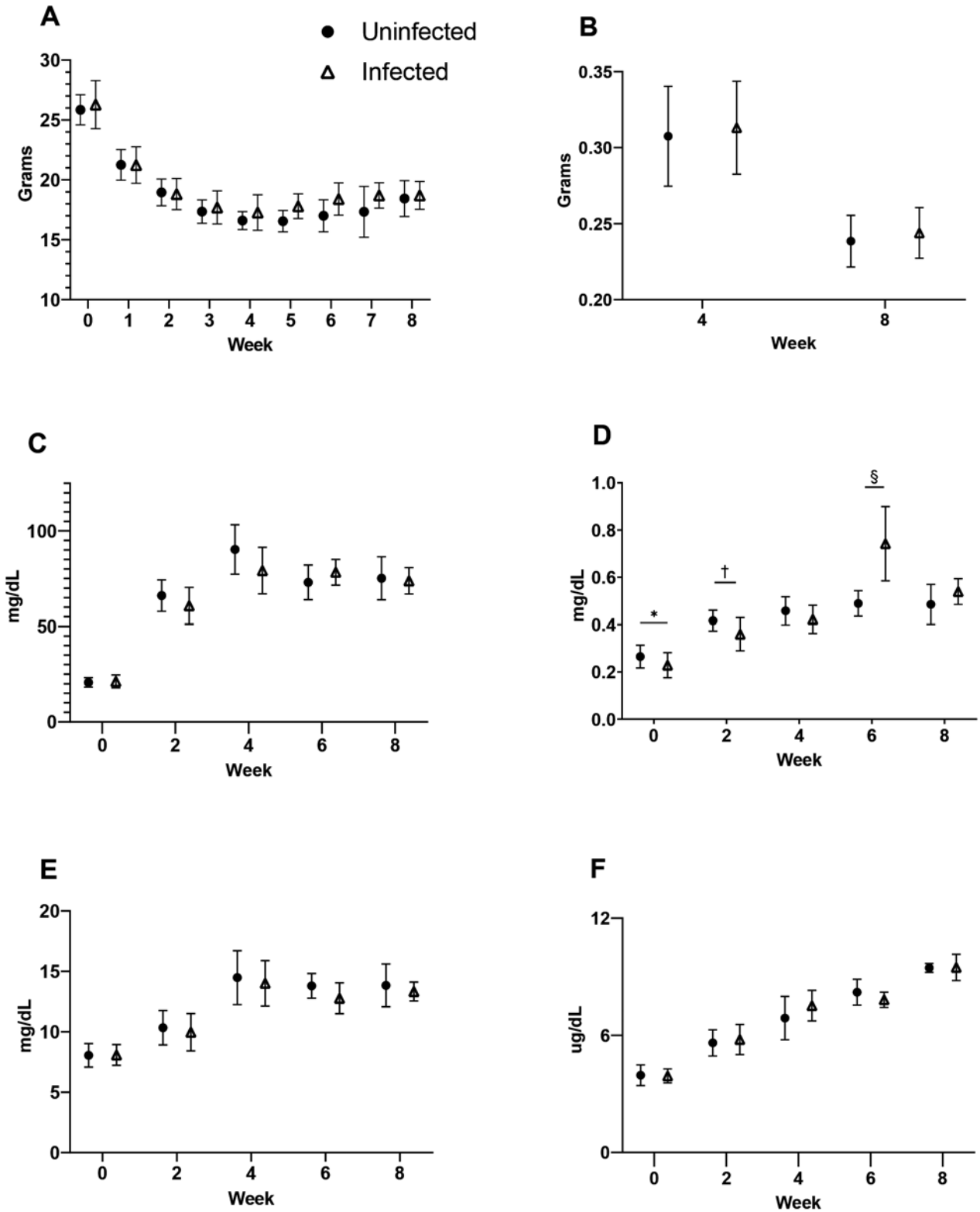

Figure 4. Body and kidney weights and serum renal function analytes in uninfected (circles) and MKPV-infected (triangles) B6 mice that consumed adenine-enriched chow for a maximum of 8 wk. Values (mean ± 1 SD) for (A) body weight, (B) combined kidney weight at time of necropsy, (C) serum BUN, (D) serum creatinine, (E) serum phosphorus, and (F) serum SDMA. *, $P < 0.05$; †, $P < 0.005$; §, $P < 0.0001$. Group size: $n = 30$ for weeks 0, 1, and 2; $n = 20$ for weeks 3 and 4; and $n = 10$ for weeks 5 through 8, except for uninfected mice at weeks 7 and 8 ($n = 8$).

results were not significantly different from the initial results. Therefore, machine error probably did not contribute to the significant difference between infected and uninfected groups at this time point. Creatinine was quantified by using the Jaffe method, which can be influenced by hemolysis, icterus, lipemia, or binding of noncreatinine chromogens.[13,55,57] Given the repeatability of the elevated creatinine, one of these factors could have affected the 6-wk blood samples from the infected group.

Table 5. Serum chemistry analytes from uninfected and MKPV-infected B6 mice fed adenine-enriched chow for 2, 4, or 8 wk

	Week 2		Week 4		Week 8	
	Uninfected	Infected	Uninfected	Infected	Uninfected	Infected
BUN (mg/dL)	71 ± 5	67 ± 11	94 ± 15	86 ± 12	75 ± 11	74 ± 7
Creatinine (mg/dL)	0.40 ± 0.10	0.39 ± 0.05	0.46 ± 0.05	0.42 ± 0.06	0.49 ± 0.08	0.54 ± 0.05
BUN:creatinine ratio	180.0 ± 28.4	172.6 ± 25.6	202.7 ± 15.5	205.5 ± 18.5	164.9 ± 70.5	137.4 ± 11.8
SDMA (µg/dL)	5.61 ± 0.7	5.78 ± 0.8	6.88 ± 1.1	7.52 ± 0.8	9.45 ± 0.2	9.48 ± 0.7
Total protein (g/dL)]	6.1 ± 0.2	6.0 ± 0.3	6.2 ± 0.5	6.0 ± 0.3	6.3 ± 0.2	6.3 ± 0.2
Albumin (g/dL)	3.2 ± 0.1	3.1 ± 0.1	3.0 ± 0.2	2.9 ± 0.1	3.2 ± 0.3	3.1 ± 0.1
Globulin (g/dL)	2.9 ± 0.2	2.9 ± 0.3	3.2 ± 0.3	3.1 ± 0.2	3.1 ± 0.2	3.2 ± 0.2
Albumin:globulin ratio	1.1 ± 0.1	1.1 ± 0.1	1.0 ± 0.1	1.0 ± 0.1	1.0 ± 0.2	1.0 ± 0.1
P (mg/dL)	11.3 ± 1.3	11.2 ± 1.6	15.6 ± 2.1	15.2 ± 1.6	13.8 ± 1.8	13.3 ± 0.8
Ca (mg/dL)	11.3 ± 0.4	11.2 ± 0.5	10.8 ± 0.5	10.9 ± 0.3	10.9 ± 1.1	11.4 ± 0.5

Data are shown as mean ± 1 SD.
Group size: n = 10 except for uninfected mice at week 8 (n = 8).

Therefore, we consider the significant difference in creatinine between infected and uninfected mice at 6 wk to an artifact.

Neither urine specific gravity, urinary creatinine, urinary total protein, nor the total urinary protein:creatinine ratio differed between infected and uninfected mice. Both infected and uninfected mice developed anemia over time; this anemia appeared to be regenerative in nature, given that both groups developed significant increases in absolute reticulocyte count over time in conjunction with significant decreases in Hct. This finding is contrary to the nonregenerative anemia that typically develops in naturally occurring CKD.[32] Previous reports of the adenine diet model have described both nonregenerative anemia and anemia with increased absolute reticulocytes, as was found in the present study.[1,2,60] The mechanism by which these mice develop a regenerative response despite profound renal injury is unclear, but our data add to the body of evidence suggesting variability in the type of anemia that develops in this model.

We were unable to determine whether serum SDMA was a more sensitive indicator of renal impairment than creatinine in the adenine diet model. In other species, as renal disease progresses, SDMA increases before serum creatinine and is therefore a more sensitive indicator of a reduction in GFR.[19,40] However, we could not document this possibility because of the rapid progression of changes. At the earliest time point, 2 wk after diet initiation, serum creatinine had already increased above the 95% percentile of the baseline serum creatinine in both groups. This rapid progression of azotemia and weight loss appears to be more severe in the present study than in previous reports involving the adenine diet.[11,23] A study evaluating earlier time points would be necessary to determine whether SDMA increases significantly in advance of creatinine. However, we did find that after initiation of the adenine diet, SDMA increased significantly from baseline and was strongly correlated with serum creatinine. Prior measurement of baseline SDMA

Table 6. Hematologic parameters from uninfected and MKPV-infected B6 mice fed adenine-enriched chow for 2, 4, or 8 wk

	Week 2		Week 4		Week 8	
	Uninfected	Infected	Uninfected	Infected	Uninfected	Infected
RBC (M/µL)	10.90 ± 2.25	10.50 ± 3.67	9.30 ± 1.25	10.26 ± 0.81	8.41 ± 1.64	9.25 ± 0.51
Hgb (g/dL)	14.7 ± 3.1	14.0 ± 4.9	11.2 ± 1.7	12.4 ± 1.1	9.0 ± 1.6	10.0 ± 0.6
Hct (%)	45.5 ± 10.9	46.2 ± 8.6	36.9 ± 6.0	41.5 ± 3.7	30.5 ± 5.3	33.8 ± 2.1
MCV (fL)	44.1 ± 1.9	43.0 ± 3.0	39.5 ± 1.5	40.4 ± 1.1	36.5 ± 2.2	36.6 ± 0.9
MCH (pg)	13.5 ± 0.4	13.2 ± 0.8	12.1 ± 0.3	12.0 ± 0.4	10.8 ± 0.4	10.8 ± 0.3
MCHC (g/dL)	30.6 ± 1.1	30.6 ± 1.4	30.5 ± 0.7	29.9 ± 0.4	29.6 ± 0.7	29.5 ± 0.7
RBC distribution width (1 SD, fL)	29.8 ± 2.0	31.0 ± 3.3	32.2 ± 3.1	32.4 ± 2.7	34.9 ± 7.2	31.5 ± 1.7
RBC distribution width (CV, %)	27.4 ± 2.7	27.8 ± 3.6	31.4 ± 2.9	31.9 ± 2.7	36.2 ± 3.2	34.0 ± 1.5
Reticulocytes (×10^3/µL)	372.9 ± 52.9	351.5 ± 204.0	468.8 ± 97.9	503.9 ± 87.4	731.5 ± 377.6	618.5 ± 85.8
Platelets (×10^3/µL)	1264 ± 388	1051 ± 832	1853 ± 290	1814 ± 335	1846 ± 600	1714 ± 642
Platelet distribution width (fL)	8.3 ± 0.5	8.5 ± 0.7	7.7 ± 0.4	7.8 ± 0.4	8.1 ± 0.5	8.1 ± 0.3
MPV (fL)	6.8 ± 0.8	6.8 ± 0.5	6.4 ± 0.9	6.6 ± 1.0	6.2 ± 1.0	5.8 ± 0.2
WBC (×10^3/µL)	9.99 ± 2.01	9.53 ± 2.51	3.54 ± 0.74	3.62 ± 0.76	4.86 ± 1.54	5.05 ± 1.58
Neutrophils (×10^3/µL)	3.51 ± 0.92	4.05 ± 1.72	2.31 ± 0.74	2.22 ± 0.44	1.82 ± 0.65	1.84 ± 0.75
Lymphocytes (×10^3/µL)	5.87 ± 1.72	4.97 ± 1.20	1.12 ± 0.47	1.29 ± 0.46	2.63 ± 1.34	2.80 ± 0.91
Monocytes (×10^3/µL)	0.46 ± 0.16	0.39 ± 0.09	0.10 ± 0.02	0.10 ± 0.05	0.35 ± 0.15	0.33 ± 0.10
Eosinophils (×10^3/µL)	0.13 ± 0.05	0.10 ± 0.06	0.01 ± 0.01	0.01 ± 0.01	0.06 ± 0.04	0.06 ± 0.04
Basophils (×10^3/µL)	0.02 ± 0.01	0.01 ± 0.01	0.01 ± 0.01	0.01 ± 0.005	0.01 ± 0.01	0.01 ± 0.01

CV, coefficient of variation
Data are shown as mean ± 1 SD.
Group size: n = 10 except for uninfected mice at week 8 (n = 8).

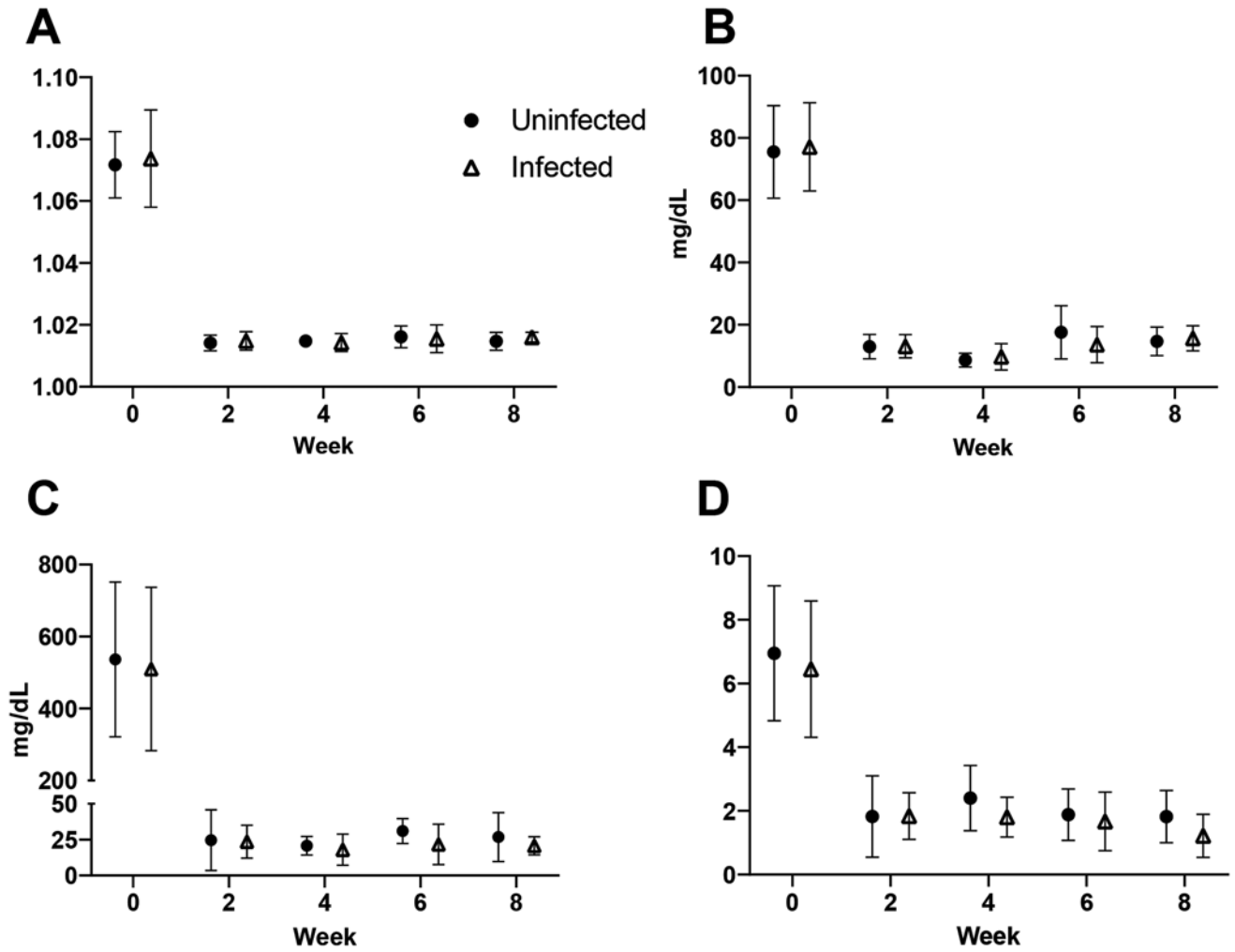

Figure 5. Urine chemistry parameters of uninfected (circles) and MKPV-infected (triangles) B6 mice that consumed adenine-enriched chow for a maximum of 8 wk. Values (mean ± 1 SD) for (A) urine specific gravity, (B) urinary creatinine, (C) urine total protein, and (D) urine total protein:creatinine ratio. Group size: $n = 30$ for weeks 0, 1, and 2; $n = 20$ for weeks 3 and 4; and $n = 10$ for weeks 5 through 8, except for uninfected mice at weeks 7 and 8 ($n = 8$).

concentrations were notably higher in male ICR mice (mean, 8.4 µg/dL) as compared with the concentrations we measured in the female C57BL/6NCrl in the present study (mean, 3.9 µg/dL); however, these differences may simply reflect differences due to strain, sex, or analytical method.[8] Additional characterization of baseline SDMA measurements in multiple strains of mice of both sexes is necessary.

Infection with MKPV causes lymphoplasmacytic interstitial inflammation in immunocompetent mice.[16] This lesion was observed in both the pharmacokinetic analyses, where MKPV-infected B6 mice had significantly higher scores for interstitial inflammation than did uninfected B6 mice regardless of the drug used, and in the adenine diet experiment, where infected mice had significantly more lymphoplasmacytic inflammatory foci than did uninfected mice at multiple time points. We hypothesized that MKPV-infected mice would develop greater interstitial fibrosis than uninfected mice because infection with MKPV has been associated with marked interstitial fibrosis in immunodeficient mice. Although prior studies of MKPV infection in immunocompetent mice have not revealed marked renal fibrosis,[38,47] the chronic inflammation that occurs in the kidneys of these mice may promote a milder form of renal fibrosis that could only be documented by stains that were not used in these studies. However, we found significantly less interstitial fibrosis at 8 wk after adenine diet initiation in mice infected with MKPV as compared with the uninfected mice. Cytokines that are known to be produced in response to viral infections, including IL10 and IFNγ, have been associated with attenuation of renal fibrosis. IL10, a multifunctional cytokine that balances the immune response by acting as a brake on inflammation, is produced by multiple types of immune cells during the acute and chronic stages of viral infections.[48] It acts to mitigate the fibrotic response in multiple organs including the kidney, based on evidence from animal models of chronic kidney disease.[56] In addition, the proinflammatory cytokine IFNγ, a key component of the antiviral immune response, inhibits renal fibrosis in experimental models.[26,42,44] If IFNγ or IL10 were elevated after MKPV infection and immune cell recruitment in immunocompetent mice, these cytokines could contribute to the attenuation of interstitial renal fibrosis observed in infected mice. Additional studies are required to determine the effects of MKPV infection on cytokine production in the kidneys of immunocompetent mice and how these effects modulate renal fibrosis.

Immunostaining for F4/80, a macrophage marker commonly used to characterize the adenine diet model, did not differ significantly between infected and uninfected mice at

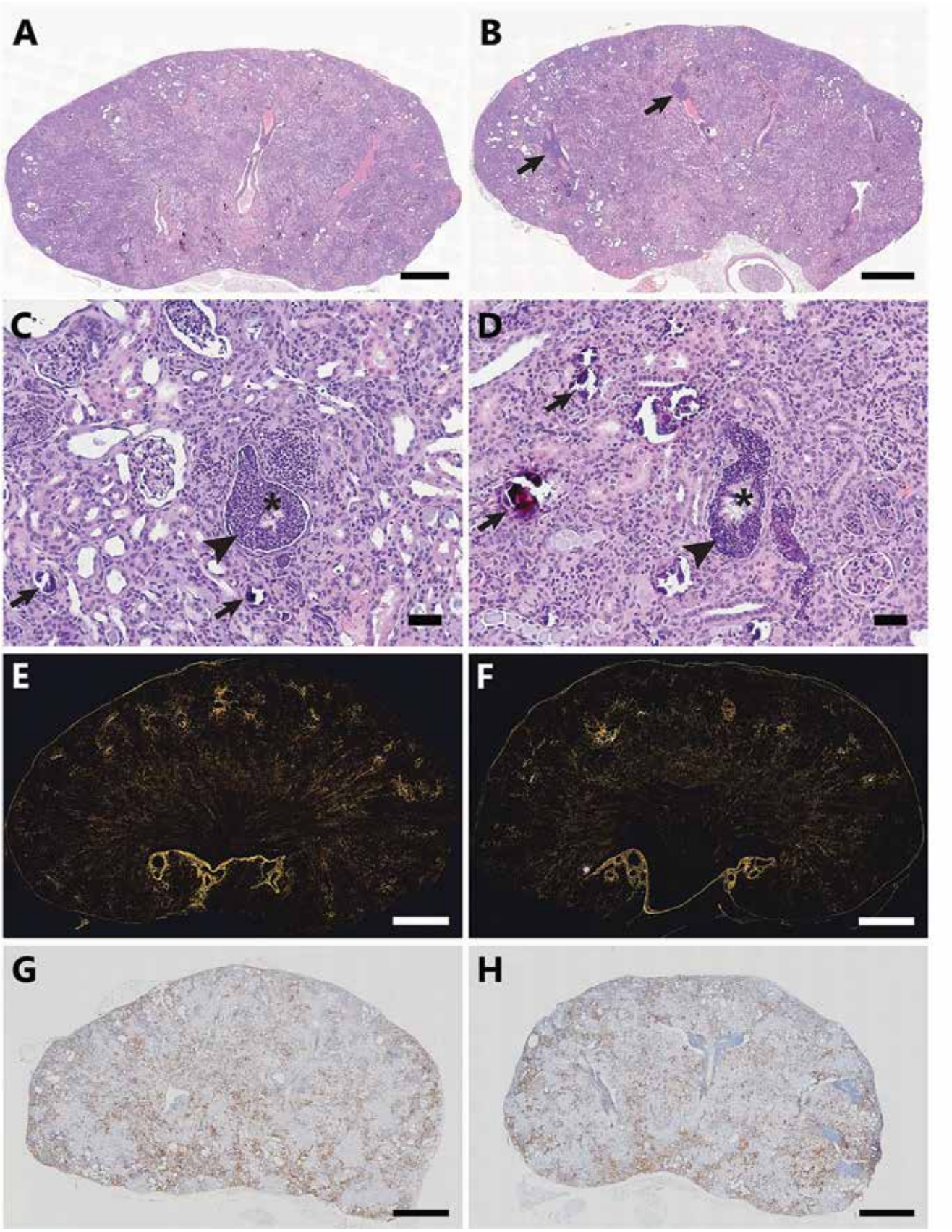

Figure 6. Representative photomicrographs of whole kidney sections from uninfected and MKPV-infected B6 mice that consumed adenine-enriched chow for 8 wk. Kidney sections demonstrating interstitial lymphoplasmacytic infiltrates (arrows) in (A) uninfected and (B) infected mice. Kidney sections demonstrating the remaining features assessed in (C) uninfected and (D) infected mice, including mineralization (arrow), intratubular inflammation (arrowhead), and adenine crystals (asterisk). Hematoxylin and eosin stain. Kidney sections photographed under polarized light demonstrating interstitial fibrosis in (E) uninfected and (F) infected mice. Sirius red stain. Kidney sections from (G) uninfected and (H) infected mice. F4/80 immunohistochemistry. Scale bars, 50 µm (C, D), 1 mm (all other panels).

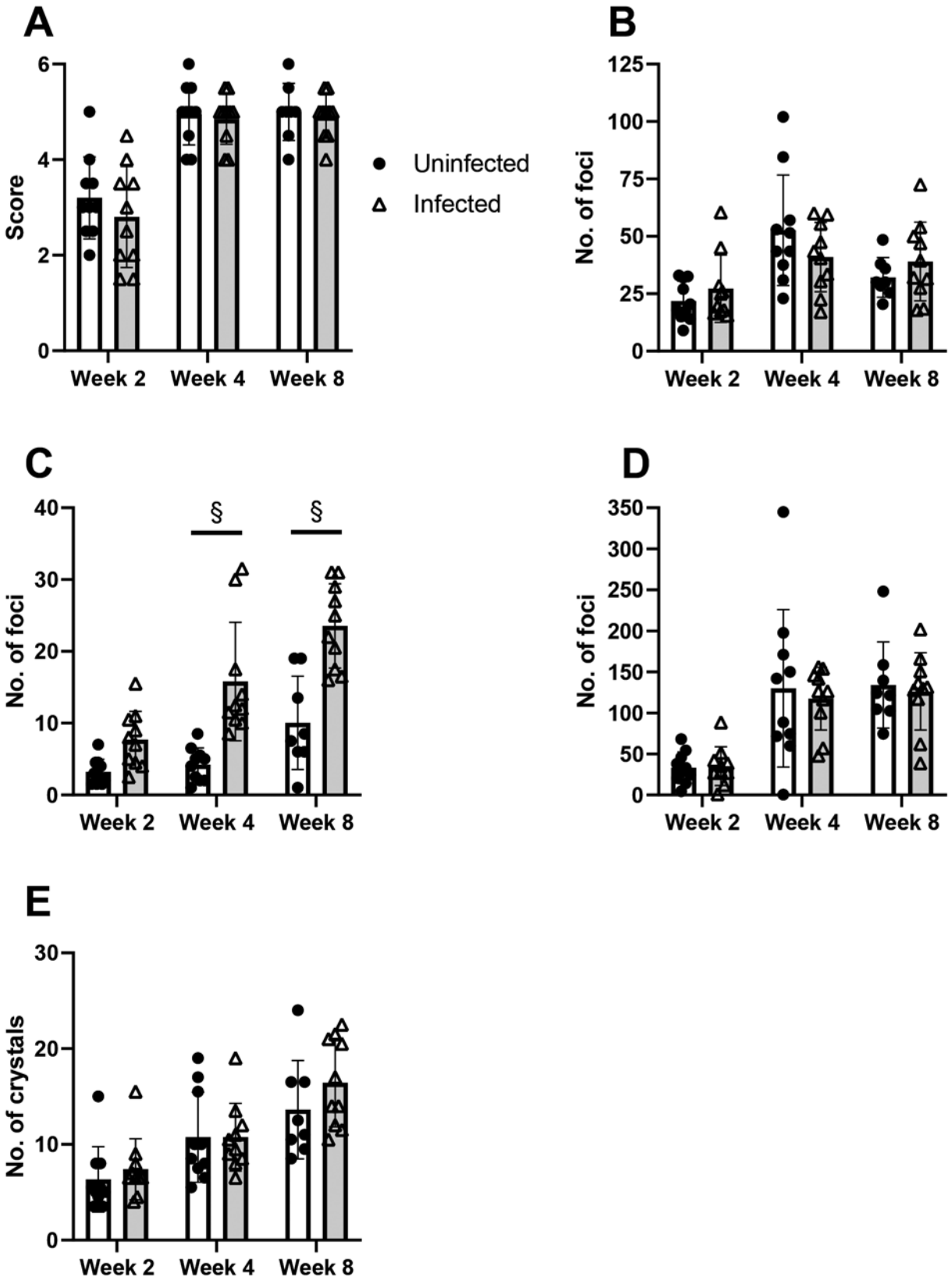

Figure 7. Histology of renal tissue from uninfected (circles) and MKPV-infected (triangles) B6 mice that consumed adenine-enriched chow for 2, 4, or 8 wk. (A) Tubular degeneration, (B) Intratubular inflammation, (C), Interstitial inflammation, (D), Mineralization, (E), Adenine crystals. Data presented as mean ± 1 SD with individual animals (symbols). All groups contained 10 mice, except for uninfected mice at week 8 (n = 8). §, $P < 0.0001$.

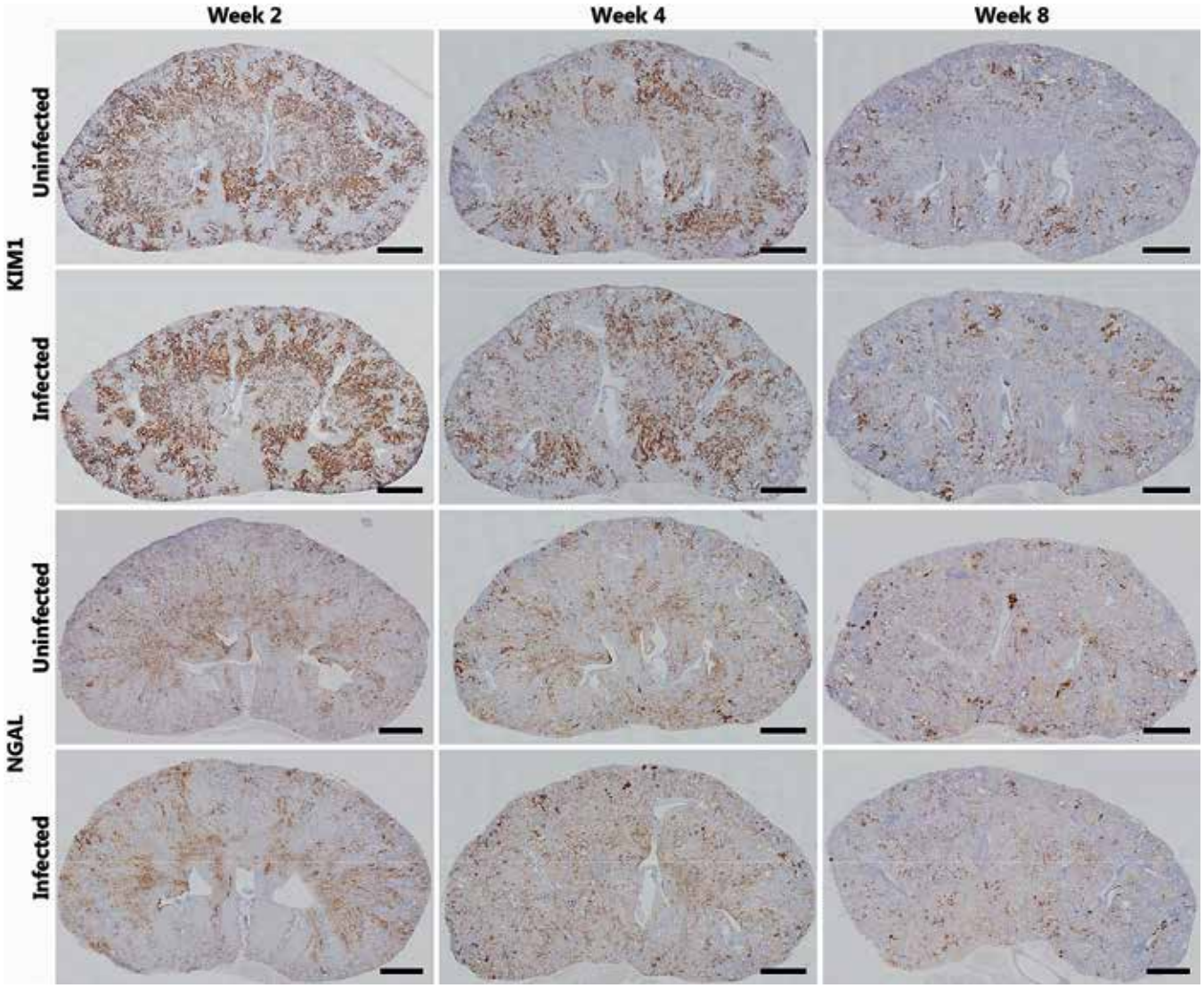

Figure 8. Representative photomicrographs of whole kidney sections from uninfected and MKPV-infected B6 mice that consumed adenine-enriched chow for 2, 4, or 8 wk: immunohistochemistry for KIM1 and NGAL Scale bars, 1 mm.

any time point. Infection with MKPV has been demonstrated to increase activated renal macrophages in immunodeficient mice.[47] This outcome may not have been apparent due to either the immunocompetency of B6 mice or subtle increases in activated renal macrophages that were obscured by the robust macrophage recruitment that occurs in the adenine diet model. Staining for kidney injury marker 1 (KIM1), a marker of renal tubular damage, has also been used to characterize renal disease in the adenine diet model but did not differ significantly between infected and uninfected mice at any time point assessed in our current study.[28,51,64] However, staining did fall over time, with kidney tissue collected after 2 wk of adenine diet consumption demonstrating significantly more staining than did tissue collected after 8 wk of adenine diet consumption. This finding is consistent with other reports showing that KIM1 mRNA expression decreased between days 7 and 14 of adenine diet consumption in wildtype C57BL/6J mice.[15] KIM1 expression is model-dependent in murine models of CKD; the unilateral ureteral obstruction model displays gradually increasing KIM1 expression over time, whereas the cisplatin model shows resolution of acute KIM1 expression by day 14 after drug administration.[61] We observed in the current study that in the adenine diet model, KIM1 expression was higher during the acute injury and declined over time. This result may reflect the temporal decrease in mass of renal tubular epithelium secondary to tubular injury. The reduction of kidney weight between weeks 4 and 8 of adenine diet consumption supports this observation. Similarly, staining for neutrophil gelatinase-associated lipocalin (NGAL), a marker of renal tubular injury in mice, was not significantly different between infected and uninfected mice at any time point.[9,65] In the present study we observed that NGAL expression declined between 2 and 8 wk after diet initiation; however, it appeared to reach peak expression at week 4, that is, later than KIM1. NGAL expression increases in injured tubular epithelial cells and is also expressed as a component of secondary granules in neutrophils[9].The latter may have contributed to the increased NGAL staining seen in our study at week 4, given that peak intratubular neutrophilic inflammation also occurred at this time.[27]

Although the results of the present study indicate that 15 wk of infection with MKPV did not significantly exacerbate the measurable clinicopathologic outcomes in the 0.2% adenine diet model of CKD, this term of infection did significantly alter select histopathologic features. However, these results cannot necessarily be extrapolated to other models of kidney disease, mouse strains, or stages of infection with the MKPV virus.

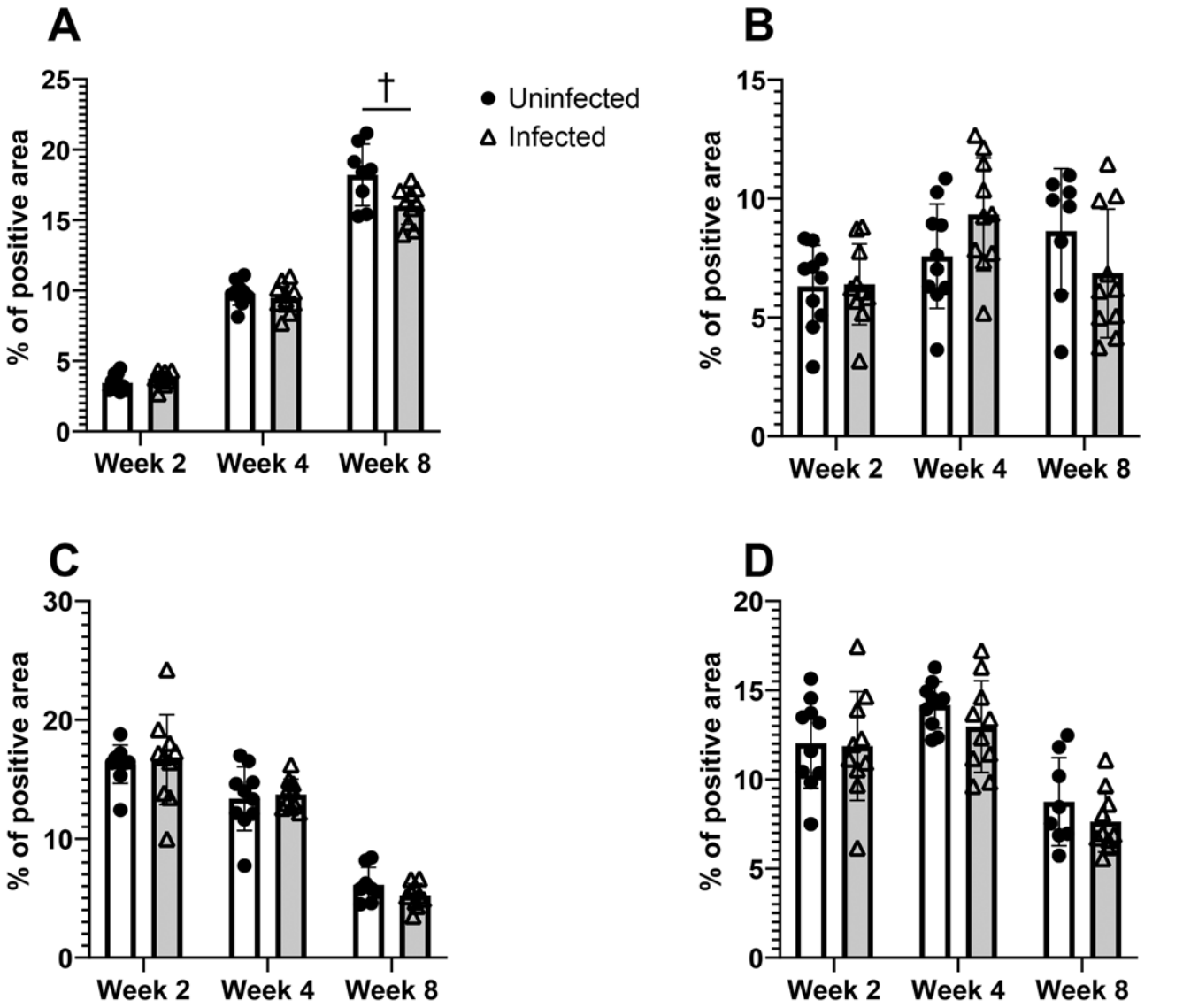

Figure 9. Proportion of renal tissue staining positive for (A) Sirius red, (B) F4/80, (C) KIM1, or (D) NGAL in uninfected (circles) and MKPV-infected (triangles) B6 mice that consumed adenine-enriched diet for 2, 4, or 8 wk. Data presented as mean ± 1 SD with individual animals (symbols) for: (A) interstitial fibrosis as determined by percentage of Sirius red–stained tissue exhibiting birefringence under polarized light, (B) F4/80-positive macrophage infiltration as determined by percentage of DAB-positive tissue, tissue injury as determined by percentage of DAB-positive tissue for (C) KIM1 or (D) NGAL. †, $P < 0.005$,. Group size: $n = 10$ except for uninfected mice at week 8 ($n = 8$).

The results of this study disproved our initial hypotheses that MKPV infection would significantly alter the renal clearance of the chemotherapeutic drugs methotrexate or lenalidomide and would alter traditional serum and urinary biomarkers of renal function in the adenine diet model of CKD. Instead, we found that after 10-15 wk of MKPV infection, NSG and B6 mice did not develop significant aberrations in their renal clearance of chemotherapeutics or clinicopathologic biomarkers of impaired renal function as compared with uninfected mice of the same strain. However, we did observe that MKPV infection altered histologic outcomes in the adenine model of CKD, and found significant inter-strain differences in methotrexate pharmacokinetics. Together, these results suggest that subclinical MKPV infection does not significantly alter renal function. However, infection with MKPV enhanced interstitial lymphoplasmacytic infiltrates and attenuated renal fibrosis at 8 wk after adenine diet initiation. Given our present results, if histologic assessment of the kidney is performed in a study using the adenine diet model, MKPV infection status should be documented and reported to enhance research reproducibility and allow comparison of results between studies. Our results also suggest that MKPV infection may confound experimental results in other models that assess renal histopathology, but further studies are required to better characterize this possibility. We did observe mouse strain–specific differences in the pharmacokinetics of the chemotherapeutics evaluated that were independent of MKPV infection. Therefore, data gathered from pharmacokinetic studies should not be extrapolated between mouse strains without validation.

Acknowledgments

This work was supported in part by the ACLAM Foundation and MSK's NCI Cancer Center Support Grant P30 CA008748. We acknowledge the contributions of Antonio Bravo, John D'Allara, Jacqueline Candelier, Kim McBride, Maria Jiao, and Iveta Simanska of the Laboratory of Comparative Pathology; Mary Leissinger (previously with

IDEXX Bioanalytics), MSK's Antitumor Assessment Core Facility, and Dr Greg Gorman (Samford University) for their assistance with the pharmacokinetics study.

References

1. **Akchurin O, Patino E, Dalal V, Meza K, Bhatia D, Brovender S, Zhu YS, Cunningham-Rundles S, Perelstein E, Kumar J, Rivella S, Choi ME.** 2019. Interleukin 6 contributes to the development of anemia in juvenile CKD. Kidney Int Rep **4**:470–483. https://doi.org/10.1016/j.ekir.2018.12.006.
2. **Akchurin O, Sureshbabu A, Doty SB, Zhu Y-S, Patino E, Cunningham-Rundles S, Choi ME, Boskey A, Rivella S.** 2016. Lack of hepcidin ameliorates anemia and improves growth in an adenine-induced mouse model of chronic kidney disease. Am J Physiol Renal Physiol **311**:F877–F889. https://doi.org/10.1152/ajprenal.00089.2016.
3. **Bankhead P, Loughrey MB, Fernández JA, Dombrowski Y, McArt DG, Dunne PD, McQuaid S, Gray RT, Murray LJ, Coleman HG, James JA, Salto-Tellez M, Hamilton PW.** 2017. QuPath: Open-source software for digital pathology image analysis. Sci Rep **7**:16878. https://doi.org/10.1038/s41598-017-17204-5.
4. **Barthold SW, Griffey SM, Percy DH.** 2016. Mouse, p 1–118. In: Barthold SW, Griffey SM, Percy DH**, eds.** Pathology of laboratory rodents and rabbits, 4th edition. Ames (IA): John Wiley & Sons.
5. **Benet LZ, Bowman CM, Sodhi JK.** 2019. How transporters have changed basic pharmacokinetic understanding. AAPS J **21**:103. https://doi.org/10.1208/s12248-019-0373-3.
6. **Center for Biologics Evaluation and Research.** 2003. [Internet]. Guidance for industry pharmacokinetics in patients with impaired hepatic function: Study design, data analysis, and impact on dosing and labeling. Food and Drug Administration. [Cited 05 July 2022]. Available at: https://www.fda.gov/media/71311/download.
7. **Center for Drug Evaluation and Research.** 2010. [Internet]. Guidance for industry M3(R2) nonclinical safety studies for the conduct of human clinical trials and marketing authorization for pharmaceuticals questions and answers, p. 5. Food and Drug Administration. [Cited 05 July 2022]. Available at: https://www.fda.gov/media/71542/download.
8. **Chae JW, Baek IH, Kang W, Kwon KI.** 2011. Simultaneous determination of L-arginine, asymmetric dimethylarginine, and symmetric dimethylarginine in the plasma of rodents with LC-MS/MS. Arzneimittelforschung **61**:340–346. https://doi.org/10.1055/s-0031-1296208.
9. **Che K, Han W, Zhang M, Niu H.** 2021. Role of neutrophil gelatinase-associated lipocalin in renal cell carcinoma (review). Oncol Lett **21**:148. https://doi.org/10.3892/ol.2020.12409.
10. **Chen N, Lau H, Kong L, Kumar G, Zeldis JB, Knight R, Laskin OL.** 2007. Pharmacokinetics of lenalidomide in subjects with various degrees of renal impairment and in subjects on hemodialysis. J Clin Pharmacol **47**:1466–1475. https://doi.org/10.1177/0091270007309563.
11. **de Frutos S, Luengo A, García-Jérez A, Hatem-Vaquero M, Griera M, O'Valle F, Rodríguez-Puyol M, Rodríguez-Puyol D, Calleros L.** 2019. Chronic kidney disease induced by an adenine rich diet upregulates integrin linked kinase (ILK) and its depletion prevents the disease progression. Biochim Biophys Acta Mol Basis Dis **1865**:1284–1297. https://doi.org/10.1016/j.bbadis.2019.01.024.
12. **de Koning BA, van Dieren JM, Lindenbergh-Kortleve DJ, van der Sluis M, Matsumoto T, Yamaguchi K, Einerhand AW, Samsom JN, Pieters R, Nieuwenhuis EE.** 2006. Contributions of mucosal immune cells to methotrexate-induced mucositis. Int Immunol **18**:941–949. https://doi.org/10.1093/intimm/dxl030.
13. **Delanghe JR, Speeckaert MM.** 2011. Creatinine determination according to Jaffe—what does it stand for? NDT Plus **4**:83–86.
14. **Dewi BE, Takasaki T, Kurane I.** 2004. In vitro assessment of human endothelial cell permeability: effects of inflammatory cytokines and dengue virus infection. J Virol Methods **121**:171–180. https://doi.org/10.1016/j.jviromet.2004.06.013.
15. **Eckes T, Patyna S, Koch A, Oftring A, Gauer S, Obermüller N, Schwalm S, Schaefer L, Chun J, Gröne H-J, Pfeilschifter J.** 2022. Sphingosine 1-Phosphate Receptor 5 (S1P5) knockout ameliorates adenine-induced nephropathy. Int J Mol Sci **23**:3952. https://doi.org/10.3390/ijms23073952.
16. **Edmondson EF, Hsieh W-T, Kramer JA, Breed MW, Roelke-Parker ME, Stephens-Devalle J, Pate NM, Bassel LL, Hollingshead MG, Karim BO, Butcher DO, Warner AC, Nagashima K, Gulani J.** 2020. Naturally acquired mouse kidney parvovirus infection produces a persistent interstitial nephritis in immunocompetent laboratory mice. Vet Pathol **57**:915–925. https://doi.org/10.1177/0300985820953500.
17. **Ernst AA, Haynes ML, Nick TG, Weiss SJ.** 1999. Usefulness of the blood urea nitrogen/creatinine ratio in gastrointestinal bleeding. Am J Emerg Med **17**:70–72. https://doi.org/10.1016/S0735-6757(99)90021-9.
18. **Grim J, Chládek J, Martínková J.** 2003. Pharmacokinetics and pharmacodynamics of methotrexate in non-neoplastic diseases. Clin Pharmacokinet **42**:139–151. https://doi.org/10.2165/00003088-200342020-00003.
19. **Hall JA, Yerramilli M, Obare E, Yerramilli M, Jewell DE.** 2014. Comparison of serum concentrations of symmetric dimethylarginine and creatinine as kidney function biomarkers in cats with chronic kidney disease. J Vet Intern Med **28**:1676–1683. https://doi.org/10.1111/jvim.12445.
20. **Hokamp JA, Nabity MB.** 2016. Renal biomarkers in domestic species. Vet Clin Pathol **45**:28–56. https://doi.org/10.1111/vcp.12333.
21. **Institute for Laboratory Animal Research.** 2011. Guide for the care and use of laboratory animals, 8th ed. Washington (DC): National Academies Press.
22. **Ivanyuk A, Livio F, Biollaz J, Buclin T.** 2017. Renal drug transporters and drug interactions. Clin Pharmacokinet **56**:825–892. https://doi.org/10.1007/s40262-017-0506-8.
23. **Jia T, Olauson H, Lindberg K, Amin R, Edvardsson K, Lindholm B, Andersson G, Wernerson A, Sabbagh Y, Schiavi S, Larsson TE.** 2013. A novel model of adenine-induced tubulointerstitial nephropathy in mice. BMC Nephrol **14**:116. https://doi.org/10.1186/1471-2369-14-116.
24. **Jung J, Seol HS, Chang S.** 2018. The generation and application of patient-derived xenograft model for cancer research. Cancer Res Treat **50**:1–10. https://doi.org/10.4143/crt.2017.307.
25. **Kain M, Monette S, Ricart Arbona R, Henderson K, Dhawan R, Monette S, Lipman N.** 2022. Infectivity and Shedding of Mouse Kidney Parvovirus After Oronasal Inoculation of C57BL/6, CD1, and NSG Mice. Comp Med **72**:376–385. https://doi.org/10.30802/AALAS-CM-22-000066.
26. **Katze MG, He Y, Gale M.** 2002. Viruses and interferon: A fight for supremacy. Nat Rev Immunol **2**:675–687. https://doi.org/10.1038/nri888.
27. **Kjeldsen L, Johnsen AH, Sengeløv H, Borregaard N.** 1993. Isolation and primary structure of NGAL, a novel protein associated with human neutrophil gelatinase. J Biol Chem **268**:10425–10432. https://doi.org/10.1016/S0021-9258(18)82217-7.
28. **Klinkhammer BM, Djudjaj S, Kunter U, Palsson R, Edvardsson VO, Wiech T, Thorsteinsdottir M, Hardarson S, Foresto-Neto O, Mulay SR, Moeller MJ, Jahnen-Dechent W, Floege J, Anders HJ, Boor P.** 2020. Cellular and molecular mechanisms of kidney injury in 2,8-dihydroxyadenine nephropathy. J Am Soc Nephrol **31**:799–816. https://doi.org/10.1681/ASN.2019080827.
29. **Latcha S.** 2016. Pharmacokinetics of chemotherapeutic agents in kidney disease, p 1–9. In: Perazella M, editor. Onco-nephrology curriculum. Washington (DC): American Scoiety of Nephrology.
30. **Lee Q, Padula MP, Pinello N, Williams SH, O'Rourke MB, Fumagalli MJ, Orkin JD, Song R, Shaban B, Brenner O, Pimanda JE, Weninger W, Souza WM, Melin AD, Wong JJ, Crim MJ, Monette S, Roediger B, Jolly CJ.** 2020. Murine and related chapparoviruses are nephro-tropic and produce novel accessory proteins in infected kidneys. PLoS Pathog **16**:e1008262. https://doi.org/10.1371/journal.ppat.1008262.
31. **Li F, Ulrich ML, Shih VF, Cochran JH, Hunter JH, Westendorf L, Neale J, Benjamin DR.** 2019. Mouse strains influence clearance and efficacy of antibody and antibody-drug conjugate via Fc-FcγR interaction. Mol Cancer Ther **18**:780–787. https://doi.org/10.1158/1535-7163.MCT-18-0977.

32. **Lippi I, Perondi F, Lubas G, Gori E, Pierini A, D'Addetta A, Marchetti V.** 2021. Erythrogram patterns in dogs with chronic kidney disease. Vet Sci **8**:123. https://doi.org/10.3390/vetsci8070123.
33. **Lobo ED, Balthasar JP.** 2003. Pharmacokinetic-pharmacodynamic modeling of methotrexate-induced toxicity in mice. J Pharm Sci **92**:1654–1664. https://doi.org/10.1002/jps.10431.
34. **Mackow ER, Gorbunova EE, Gavrilovskaya IN.** 2015. Endothelial cell dysfunction in viral hemorrhage and edema. Front Microbiol **5**:733.
35. **Malaney P, Nicosia SV, Davé V.** 2014. One mouse, one patient paradigm: New avatars of personalized cancer therapy. Cancer Lett **344**:1–12. https://doi.org/10.1016/j.canlet.2013.10.010.
36. **Mansoor A, Mahabadi, N.** 2022. Volume of distribution. Treasure Island (FL): StatPearls Publishing.
37. **Martinez MN, Greene J, Kenna L, Kissell L, Kuhn M.** 2020. The impact of infection and inflammation on drug metabolism, active transport, and systemic drug concentrations in veterinary species. Drug Metab Dispos **48**:631–644. https://doi.org/10.1124/dmd.120.090704.
38. **Meng X-M, Nikolic-Paterson DJ, Lan HY.** 2014. Inflammatory processes in renal fibrosis. Nat Rev Nephrol **10**:493–503. https://doi.org/10.1038/nrneph.2014.114.
39. **Michaud SA, Sinclair NJ, Pětrošová H, Palmer AL, Pistawka AJ, Zhang S, Hardie DB, Mohammed Y, Eshghi A, Richard VR, Sickmann A, Borchers CH.** 2018. Molecular phenotyping of laboratory mouse strains using 500 multiple reaction monitoring mass spectrometry plasma assays. Commun Biol **1**:78. https://doi.org/10.1038/s42003-018-0087-6.
40. **Nabity MB, Lees GE, Boggess MM, Yerramilli M, Obare E, Yerramilli M, Rakitin A, Aguiar J, Relford R.** 2015. Symmetric dimethylarginine assay validation, stability, and evaluation as a marker for the early detection of chronic kidney disease in dogs. J Vet Intern Med **29**:1036–1044. https://doi.org/10.1111/jvim.12835.
41. **Okada S, Vaeteewoottacharn K, Kariya R.** 2019. Application of highly immunocompromised mice for the establishment of patient-derived xenograft (PDX) models. Cells **8**:889. https://doi.org/10.3390/cells8080889.
42. **Oldroyd SD, Thomas GL, Gabbiani G, El Nahas AM.** 1999. Interferon-gamma inhibits experimental renal fibrosis. Kidney Int **56**:2116–2127. https://doi.org/10.1046/j.1523-1755.1999.00775.x.
43. **Pénzes JJ, Söderlund-Venermo M, Canuti M, Eis-Hübinger AM, Hughes J, Cotmore SF, Harrach B.** 2020. Reorganizing the family *Parvoviridae*: A revised taxonomy independent of the canonical approach based on host association. Arch Virol **165**:2133–2146. https://doi.org/10.1007/s00705-020-04632-4.
44. **Poosti F, Bansal R, Yazdani S, Prakash J, Post E, Klok P, van den Born J, de Borst MH, van Goor H, Poelstra K, Hillebrands JL.** 2015. Selective delivery of IFNγ to renal interstitial myofibroblasts: A novel strategy for the treatment of renal fibrosis. FASEB J **29**:1029–1042. https://doi.org/10.1096/fj.14-258459.
45. **Rahman A, Yamazaki D, Sufiun A, Kitada K, Hitomi H, Nakano D, Nishiyama A.** 2018. A novel approach to adenine-induced chronic kidney disease associated anemia in rodents. PLoS One **13**:e0192531. https://doi.org/10.1371/journal.pone.0192531.
46. **Ricart Arbona RJ, Kelly S, Wang C, Dhawan RK, Henderson KS, Shek WR, Williams SH, Altan E, Delwart E, Wolf F, Lipman NS.** 2020. Serendipitous discovery of a novel murine astrovirus contaminating a murine helper T-cell line and incapable of infecting highly immunodeficient mice. Comp Med **70**:359–369. https://doi.org/10.30802/AALAS-CM-19-000106.
47. **Roediger B, Lee Q, Tikoo S, Cobbin JCA, Henderson JM, Jormakka M, O'Rourke MB, Padula MP, Pinello N, Henry M, Wynne M, Santagostino SF, Brayton CF, Rasmussen L, Lisowski L, Tay SS, Harris DC, Bertram JF, Dowling JP, Bertolino P, Lai JH, Wu W, Bachovchin WW, Wong JJL, Gorrell MD, Shaban B, Holmes EC, Jolly CJ, Monette S, Weninger W.** 2018. An atypical parvovirus drives chronic tubulointerstitial nephropathy and kidney fibrosis. Cell **175**:530–543. https://doi.org/10.1016/j.cell.2018.08.013.
48. **Rojas JM, Avia M, Martín V, Sevilla N.** 2017. IL-10: A multifunctional cytokine in viral infections. J Immunol Res **2017**:6104054. https://doi.org/10.1155/2017/6104054.
49. **Rozewski DM, Herman SE, Towns WH 2nd, Mahoney E, Stefanovski MR, Shin JD, Yang X, Gao Y, Li X, Jarjoura D, Byrd JC, Johnson AJ, Phelps MA.** 2012. Pharmacokinetics and tissue disposition of lenalidomide in mice. AAPS J **14**:872–882. https://doi.org/10.1208/s12248-012-9401-2.
50. **Santana AC, Degaspari S, Catanozi S, Dellê H, de Sá Lima L, Silva C, Blanco P, Solez K, Scavone C, Noronha IL.** 2013. Thalidomide suppresses inflammation in adenine-induced CKD with uraemia in mice. Nephrol Dial Transplant **28**:1140–1149. https://doi.org/10.1093/ndt/gfs569.
51. **Schley G, Klanke B, Kalucka J, Schatz V, Daniel C, Mayer M, Goppelt-Struebe M, Herrmann M, Thorsteinsdottir M, Palsson R, Beneke A, Katschinski DM, Burzlaff N, Eckardt K-U, Weidemann A, Jantsch J, Willam C.** 2019. Mononuclear phagocytes orchestrate prolyl hydroxylase inhibition-mediated renoprotection in chronic tubulointerstitial nephritis. Kidney Int **96**:378–396. https://doi.org/10.1016/j.kint.2019.02.016.
52. **Sedgwick JB, Menon I, Gern JE, Busse WW.** 2002. Effects of inflammatory cytokines on the permeability of human lung microvascular endothelial cell monolayers and differential eosinophil transmigration. J Allergy Clin Immunol **110**:752–756. https://doi.org/10.1067/mai.2002.128581.
53. **Shultz LD, Lyons BL, Burzenski LM, Gott B, Chen X, Chaleff S, Kotb M, Gillies SD, King M, Mangada J, Greiner DL, Handgretinger R.** 2005. Human lymphoid and myeloid cell development in NOD/LtSz-scid IL2R gamma null mice engrafted with mobilized human hemopoietic stem cells. J Immunol **174**:6477–6489. https://doi.org/10.4049/jimmunol.174.10.6477.
54. **Smith DA, Di L, Kerns EH.** 2010. The effect of plasma protein binding on in vivo efficacy: misconceptions in drug discovery. Nat Rev Drug Discov **9**:929–939. https://doi.org/10.1038/nrd3287.
55. **Srisawasdi P, Chaichanajarernkul U, Teerakanjana N, Vanavanan S, Kroll MH.** 2010. Exogenous interferences with Jaffe creatinine assays: Addition of sodium dodecyl sulfate to reagent eliminates bilirubin and total protein interference with Jaffe methods. J Clin Lab Anal **24**:123–133. https://doi.org/10.1002/jcla.20350.
56. **Steen EH, Wang X, Balaji S, Butte MJ, Bollyky PL, Keswani SG.** 2020. The role of the anti-inflammatory cytokine interleukin-10 in tissue fibrosis. Adv Wound Care (New Rochelle) **9**:184–198. https://doi.org/10.1089/wound.2019.1032.
57. **Syme NR, Stevens K, Stirling C, McMillan DC, Talwar D.** 2020. Clinical and analytical impact of moving from Jaffe to enzymatic serum creatinine methodology. J Appl Lab Med **5**:631–642. https://doi.org/10.1093/jalm/jfaa053.
58. **Tamura M, Aizawa R, Hori M, Ozaki H.** 2009. Progressive renal dysfunction and macrophage infiltration in interstitial fibrosis in an adenine-induced tubulointerstitial nephritis mouse model. Histochem Cell Biol **131**:483–490. https://doi.org/10.1007/s00418-009-0557-5.
59. **Tani T, Orimo H, Shimizu A, Tsuruoka S.** 2017. Development of a novel chronic kidney disease mouse model to evaluate the progression of hyperphosphatemia and associated mineral bone disease. Sci Rep **7**:2233. https://doi.org/10.1038/s41598-017-02351-6.
60. **Thibodeau JF, Simard JC, Holterman CE, Blais A, Cloutier MP, Medeiros T, Leduc M, Grouix B, Leblond FA, Burger D, Hébert RL, Kennedy CRJ, Gagnon L.** 2019. PBI-4050 via GPR40 activation improves adenine-induced kidney injury in mice. Clin Sci (Lond) **133**:1587–1602. https://doi.org/10.1042/CS20190479.
61. **Tian L, Shao X, Xie Y, Wang Q, Che X, Zhang M, Xu W, Xu Y, Mou S, Ni Z.** 2017. Kidney injury molecule-1 is elevated in nephropathy and mediates macrophage activation via the mapk signalling pathway. Cell Physiol Biochem **41**:769–783. https://doi.org/10.1159/000458737.
62. **Tsukada T, Nakano T, Miyata T, Sasaki S.** 2013. Life-threatening gastrointestinal mucosal necrosis during methotrexate treatment for rheumatoid arthritis. Case Rep Gastroenterol **7**:470–475. https://doi.org/10.1159/000356817.
63. **Tucker GT.** 1981. Measurement of the renal clearance of drugs. Br J Clin Pharmacol **12**:761–770. https://doi.org/10.1111/j.1365-2125.1981.tb01304.x.
64. **van Timmeren MM, Bakker SJ, Vaidya VS, Bailly V, Schuurs TA, Damman J, Stegeman CA, Bonventre JV, van Goor H.** 2006. Tubular kidney injury molecule-1 in protein-overload nephropathy. Am J Physiol Renal Physiol **291**:F456–F464. https://doi.org/10.1152/ajprenal.00403.2005.

65. **Viau A, El Karoui K, Laouari D, Burtin M, Nguyen C, Mori K, Pillebout E, Berger T, Mak TW, Knebelmann B, Friedlander G, Barasch J, Terzi F.** 2010. Lipocalin 2 is essential for chronic kidney disease progression in mice and humans. J Clin Invest **120**:4065–4076. https://doi.org/10.1172/JCI42004.
66. **Yu J, Zhou Z, Tay-Sontheimer J, Levy RH, Ragueneau-Majlessi I.** 2018. Risk of clinically relevant pharmacokinetic-based drug-drug interactions with drugs approved by the U.S. Food and Drug Administration between 2013 and 2016. Drug Metab Dispos **46**:835–845. https://doi.org/10.1124/dmd.117.078691.
67. **Zhan M, Yang R, Wang H, He M, Chen W, Xu S, Yang L, Liu Q, Long M, Wang J.** 2018. Guided chemotherapy based on patient-derived mini-xenograft models improves survival of gallbladder carcinoma patients. Cancer Commun (Lond) **38**:48. https://doi.org/10.1186/s40880-018-0318-8.
68. **Zhao Y, Liu P, Xin Z, Shi C, Bai Y, Sun X, Zhao Y, Wang X, Liu L, Zhao X, Chen Z, Zhang H.** 2019. Biological characteristics of severe combined immunodeficient mice produced by CRISPR/Cas9-mediated Rag2 and IL2rg mutation. Front Genet **10**:401. https://doi.org/10.3389/fgene.2019.00401.